Chapter 8
Neurological Analyses: Focus on Gangliosides and Mass Spectrometry

Alina D. Zamfir

Abstract Gangliosides, sialylated glycosphingolipids, are particularly enriched in mammalian central nervous system where their expression is cell type-specific and changes particularly during brain development, maturation, aging, and diseases. For this reason, gangliosides are important diagnostic markers for various brain ailments, including primary and secondary brain tumors and neurodegenerative diseases. Among all biochemical and biophysical methods employed so far for ganglioside analysis, mass spectrometry (MS) emerged as one of the most reliable due to the sensitivity, accuracy, and speed of analysis as well as the possibility to characterize in details the molecular structure of the identified biomarkers.

This chapter presents significant achievements of MS with either electrospray (ESI), chip-based ESI, or matrix-assisted laser desorption/ionization (MALDI) in the analysis of gangliosides in normal and diseased human brain. Specifically, the chapter assesses the MS contribution in determination of topospecificity, filogenetic, and brain development stage dependence of ganglioside composition and structure as well as in discovery of ganglioside markers in neurodegenerative/neurodevelopmental conditions, primary and secondary brain tumors. The highlighted accomplishments in characterization of novel structures associated to severe brain pathologies show that MS has real perspectives to become a routine method for early diagnosis and therapy based on this biomolecule class.

A.D. Zamfir (✉)
Faculty of Physics, West University of Timisoara, 4 Boulevard V. Parvan, Timisoara, Romania

National Institute for Research and Development in Electrochemistry and Condensed Matter, 1 P. Andronescu Street, Timisoara, Romania
e-mail: alina.zamfir@uav.ro

A.G. Woods and C.C. Darie (eds.), *Advancements of Mass Spectrometry in Biomedical Research*, Advances in Experimental Medicine and Biology 806,
DOI 10.1007/978-3-319-06068-2_8,

8.1 Introduction

Lipid bilayer membranes of the vertebrate cells contain a special class of glycosphingolipids (GSL) called gangliosides. Gangliosides consist of a hydrophobic ceramide (Cer) moiety through which the molecule is attached to the plasma membrane and a hydrophilic oligosaccharide chain. Cer includes a sphingoid base and a fatty acid chain, both with variable composition from a species to another. The carbohydrate core also exhibits variability of the length and structure. Besides, one or more characteristic sialic acid groups (i.e., *N*-acetylneuraminic acid, *N*-glycolylneuraminic acid) are attached to the oligosacchride core by an aketosidic linkage. This way, gangliosides are inserted in the outer layer of the plasma membrane [56] via the heterogeneous ceramide moiety, while their oligosaccharide chain faces the external medium; thus, the carbohydrate chain is free to interact with soluble extracellular molecules and with the hydrophilic portion of other membrane components.

Although this particular class of GSLs is expressed on basically all vertebrate cells, systematic investigations showed that central nervous system (CNS) contains a several times higher ganglioside concentration than the extraneural tissue. This feature indicates that ganglioside molecules are of particular importance for the development and function of CNS [58].

As plasma-membrane components, enriched in specialized microdomains, i.e., "glycosynapse," gangliosides interact with different signal transducers, thus mediating carbohydrate-dependent cell adhesion and inducing cell activation, motility, and growth. Several reports emphasize the participation of gangliosides in significant biological processes in the healthy CNS such as brain development, maturation, aging [58], and defined functions of each specialized brain region, as well as in pathological CNS, in particular neurodegenerative diseases [59] and malignant transformation [26]. The regulatory roles of gangliosides at the CNS level were clearly demonstrated by the observed dramatic change in their expression and structure during development of the nervous system and their region-specific distribution. On the other hand, certain structures were found to be differentially and specifically expressed in the brain affected by neurodegenerative diseases [77]. Changes in ganglioside composition and content have been observed also during neoplastic cell transformation. A decrease in the regular ganglioside profile and an increase in the structures detected only in small amounts in the normal brain tissue were found in primary and secondary (metastases) brain tumors, demonstrating a direct correlation between ganglioside composition and histological type and grade of the tumors [9, 17, 66]. This aspect provides the option to use gangliosides as biochemical markers in early histopathological diagnosis, grading, and prognosis of tumors. Therefore, nowadays gangliosides are considered valuable diagnostic markers of CNS ailments being in the current focus of research also as potential therapeutic agents.

In the last decade several biophysical methods have been developed for the investigation of ganglioside expression in severe brain diseases. Hence, for the assessment of ganglioside quantity and composition in human brain, cell- and tissue-staining analyses such as immunocytochemistry and immunohistochemistry and assays using chromatographic methods based on thin layer chromatography (TLC) and high-performance liquid chromatography (HPLC) were successfully employed [40, 69]. Ganglioside profiling, their quantification, and correlation to histomorphology and grading of human tumors, i.e., gliomas, were studied using a newly developed microbore HPLC method [84]. Also, the application of infrared spectroscopy as an adjunct to histopathology in detecting and diagnosing human brain tumors was demonstrated [36, 70]. Also, ganglioside expression in human glioblastoma was determined by confocal microscopy of immunostained brain sections using antiganglioside monoclonal antibodies [27]. However, to define the structure-to-function interrelationship of each particular ganglioside implicated in a physiological/pathological process and to improve their diagnostic significance, more sensitive and accurate approaches to enhance lipid-linked carbohydrate analysis under high-structural complexity were necessary. In this context, mass spectrometry (MS) has emerged lately as one of the most potent tools for the structural analysis of complex brain gangliosides. Implemented initially with fast atom bombardment (FAB) ionization [15], the capability of MS for sensitive structural analysis of gangliosides increased significantly after the introduction of matrix-assisted laser desorption / ionization (MALDI) and electrospray (ESI) ionization from one side and the possibility to perform tandem MS or multistage MS for detailed structural analysis.

Nevertheless, as compared to other classes of biomolecules, mass spectrometry of gangliosides has developed much slower. Although the value of ganglioside markers is universally acknowledged, the current inventory of species identified by MS is rather poor as compared to proteomics field, and the number of research laboratories constantly involved in MS of gangliosides is reduced to only a few, worldwide. This state-of-the-art is a result of the high structural diversity and heterogeneity of gangliosides and their inferior ionization efficiency as compared to peptides and proteins, which require reconsideration of all MS conditions for screening and sequencing. The experimental design must also be adapted to the type of the possibly present labile moieties (NeuAc, Fuc, *O*-Ac), the ionizability of the functional groups, and the special molecule constitution consisting of a hydrophilic sugar core and a hydrophobic ceramide part. All these characteristics made the class of gangliosides less amenable to MS. However, in the subsequent parts of this chapter it will be shown that adequate strategies may lead to a successful implementation of MS in ganglioside analysis, with important results not only in brain mapping but also in discovery of species associated to severe brain diseases.

8.2 Ganglioside Nomenclature

Gangliosides and the precursor glycosphingolipids are currently abbreviated according to the system introduced by Svennerholm and Fredman [71] and the recommendations of IUPAC-IUB Commission on Biochemical Nomenclature [30] as follows: LacCer, Galβ4Glcβ1Cer; GA2, Gg_3Cer, GalNAcβ4Galβ4Glcβ1Cer; GA1, Gg_4Cer, Galβ3GalNAcβ4Galβ4Glcβ1Cer; nLc_4Cer, Galβ4GlcNAcβ3Galβ4Glcβ1Cer; Lc_4Cer, Galβ3GlcNAcβ3Galβ4Glcβ1Cer; GM3, II^3-α-Neu5Ac-LacCer; GD3, II^3-α-$(Neu5Ac)_2$- LacCer; GT3, II^3-α-$(Neu5Ac)_{3\text{-}LacCer}$; GM2, II^3-α-Neu5Ac-Gg_3Cer; GD2, II^3-α-$(Neu5Ac)_2$-Gg_3Cer; GM1a or GM1, II^3-α-Neu5Ac-Gg_4Cer; GM1b, IV^3-α-Neu5Ac-Gg_4Cer; GalNAc-GM1b, IV^3-α-Neu5Ac-Gg5Cer; GD1a, IV^3-α-Neu5Ac,II^3-α-Neu5Ac-Gg_4Cer; GD1b, II^3-α-$(Neu5Ac)_2$-Gg_4Cer; GT1b, IV^3-α-Neu5Ac,II^3-α-$(Neu5Ac)_2$-Gg_4Cer; GQ1b, IV^3-α-$(Neu5Ac)_2$,II^3-α-$(Neu5Ac)_2$-Gg_4Cer; nLM1 or 3′-nLM1, IV^3-α-Neu5Ac-nLc4Cer; LM1 or 3′-isoLM1, IV^3-α-Neu5Ac-Lc_4Cer; nLD1, disialo-nLc_4Cer;

8.3 Gangliosides in Normal Brain

Prior to MS introduction in brain research, mapping of the gangliosides expressed in different regions of normal human brain was carried out using high affinity anti-ganglioside antibodies based on immunohistochemistry, TLC coupled with densitometric scanning and two-dimensional TLC. Because of the principle of detection, restricted to major components, and the low throughput, these methods offered a limited amount of information. Therefore, in last years many efforts to implement mass spectrometry with either ESI, nanoESI chip, or MALDI methodologies into CNS ganglioside analysis have been invested.

8.3.1 Cerebrum

In view of the technical performances and the accuracy of data with biological impact, high-resolution mass spectrometry on either Fourier transform ion cyclotron resonance (FTICR) MS or quadruple time of-flight (QTOF) MS proved a remarkable potential in brain ganglioside research. In comparison to all other MS methods, FTICR MS exhibits an ultra-high resolution exceeding 10^6 and a mass accuracy often below 1 ppm [53]. FTICR MS provides at the same time the advantage of several ion fragmentation techniques based on precursor dissociation such as CID, sustained off-resonance irradiation (SORI-CID), infrared laser multiphoton (IRMPD), or electron capture dissociation (ECD) as well as the possibility to perform multiple stage MS (MS^n).

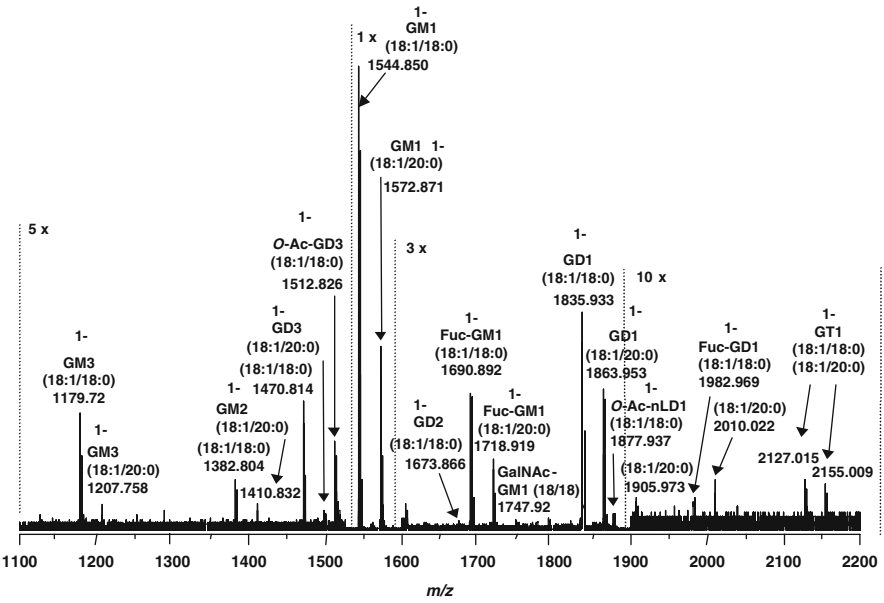

Fig. 8.1 NanoESI FTICR MS in negative ion mode of the ganglioside mixture from normal adult human cerebrum. Solvent Methanol. Sample concentration 5 pmol/μL. Capillary exit voltage 150 V. Number of scans 150. (Zamfir, Vukelić et al. unpublished results)

In brain ganglioside research nanoESI FTICR MS in the negative ion mode was shown [81] to be highly effective for screening and sequencing of the native ganglioside mixture extracted from human cerebrum (Fig. 8.1), for detailed structural analysis of an isolated GT1 (d18:1/20:0) fraction screened by nanoESI (Fig. 8.2) and sequenced using SORI-CID (Fig. 8.3). It was found that instrumental set-up in negative ion mode detection and the solvent systems play a critical role for ganglioside ion formation by nanoESI FTICR MS and for generation in SORI-CID MS^2 of product ions diagnostic for the polysialylated species.

Under adequate nanoESI FTICR MS screening conditions, cerebrum-associated ganglioside species decorated with labile attachments that readily cleave-off such as *O*-fucosylation and *O*-acetylation were detected in intact form (Fig. 8.1). Moreover, under thoroughly optimized SORI settings a set of fragment ions specific for the GT1 molecular form carrying the disialo ($Neu5Ac_2$) element at the inner galactose (Gal) residue were generated. Such a configuration is consistent with the GT1b (d18:1/20:0) isomer in human cerebrum, identified under an average mass accuracy below 5 ppm, at a sample concentration of only 5 pmol/μL. This enhancement of the sensitivity is of particular importance for characterization of material from biological sources wherefrom only minute quantities are available.

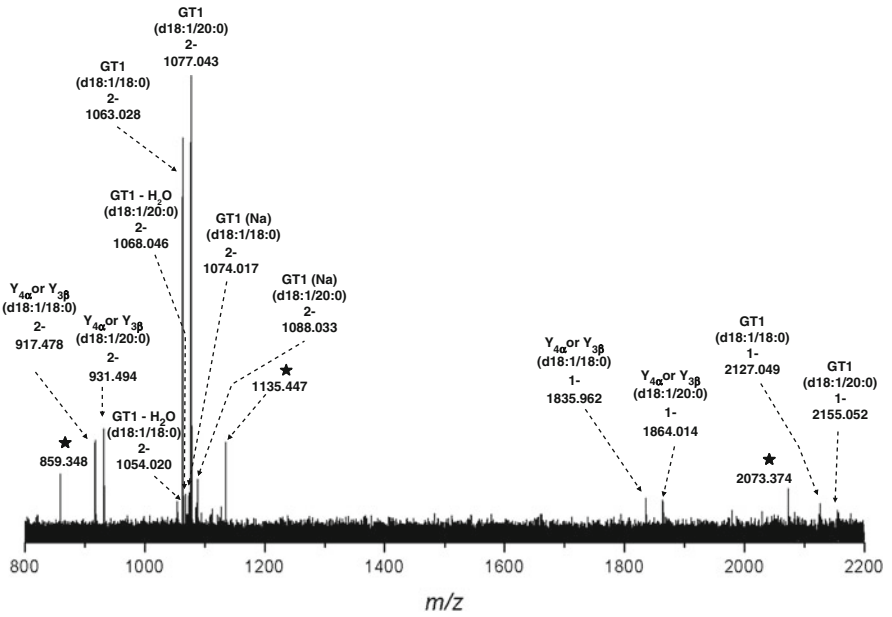

Fig. 8.2 NanoESI FTICR MS in negative ion mode of the purified GT1 fraction from normal adult human brain. Conditions as in Fig. 8.1. The assignment of the *in-source* fragmented ions is according to the nomenclature [14]. Reprinted with permission from Vukelić et al. [81]

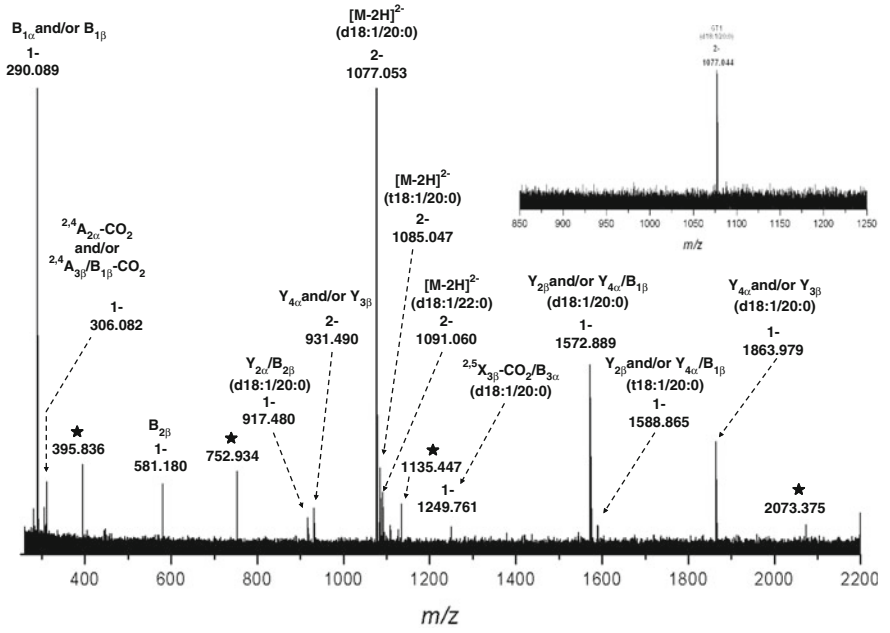

Fig. 8.3 NanoESI-FTICR SORI-CID MS^2 in negative ion mode of the doubly deprotonated molecule at *m/z* 1,077.043 corresponding to GT1 (d18:1/20:0) ganglioside species in human brain. Inset: Isolation of the precursor ion. Excitation pulse length 0.4 s. Collision gas Ar. Other conditions as in Fig. 8.1. The assignment of the fragment ions is according to the nomenclature [14]. Reprinted with permission from Vukelić et al. [81]

8.3.2 Cerebellum

Cerebellum is a morpho-anatomically and functionally highly specialized region of the brain with characteristic differences in the composition of its major ganglioside species, in comparison with cerebrum. The function, behavior, and even survival of cerebellar neurons are highly dependant on the cellular expression of the ganglioside species.

The first exhaustive determination of ganglioside expression in human cerebellum was accomplished by mass spectrometry using a high-resolution instrument (QTOF MS) in combination with silicon chip-based nanoESI [88]. Due to highly efficient ionization properties, silicon-based chips for nanoESI incorporated in a NanoMate robot (Advion Biosciences) preferentially form multiply charged ions. Furthermore, the *in-source* fragmentation of labile groups attached to the biomolecular core is minimized. With an internal diameter of the nozzle of 2.5 μm the system allows for flow rates down to 30–50 nL/min which represents a gain in sensitivity by at least five times as compared to classical nanospray capillaries. Additionally, the nozzles on the ESI chip provide a long-lasting steady spray, and elimination of sample-to-sample carryover.

In view of these advantages NanoMate incorporating chip ESI technology was coupled to QTOF MS and MS/MS and optimized in the negative ion mode, for the characterization of a complex cerebellar ganglioside mixture [88]. Negative ion mode screening of the cerebellum gray matter extracts enabled the identification of no less than 46 different ganglioside species exhibiting high heterogeneity in the ceramide motifs, sialylation status, and biologically relevant modifications (Fig. 8.4a, b, Table 8.1). This way, the first realistic representation of the ganglioside complexity, when compared against TLC and capillary-based ESI, was achieved. The mixture was found dominated by GD1 glycoforms: 19 different doubly deprotonated molecular variants of GD1 have been detected. Also identified in the mixture were GM1, GM2, GM3, GD2, GD3, GT1, and GQ1, expressing different ceramide portions. Biologically interesting *O*-acetylated and/or fucosylated GM1, GD1, GT1, and GQ1 exhibiting a high degree of heterogeneity in their ceramide motifs were also discovered (Table 8.1). For the first time, fully automated nanoESI chip MS infusion was combined also with automated precursor ion selection and fragmentation in data-dependant acquisition, allowing to obtain a sufficient set of "fingerprint" ions for the structural elucidation of a GT1b isomer having the configuration (d18:1/18:0), within 1 min of acquiring MS/MS data and only approximately 0.5 pmol of sample consumption.

In combination with ion trap mass spectrometry, chip-based nanoESI system was also used for determination of gangliosides expressed in fetal cerebellum [49]. A number of 56 ganglioside and asialo ganglioside species differing in either the composition of the glycan core and/or that of the ceramide were identified. Interestingly, *O*-Ac- and/or Fuc-modified gangliosides, found in the adult human cerebellum, were not identified in fetal human cerebellum. Ganglioside chains modified by such attachments are associated with the tissue during its

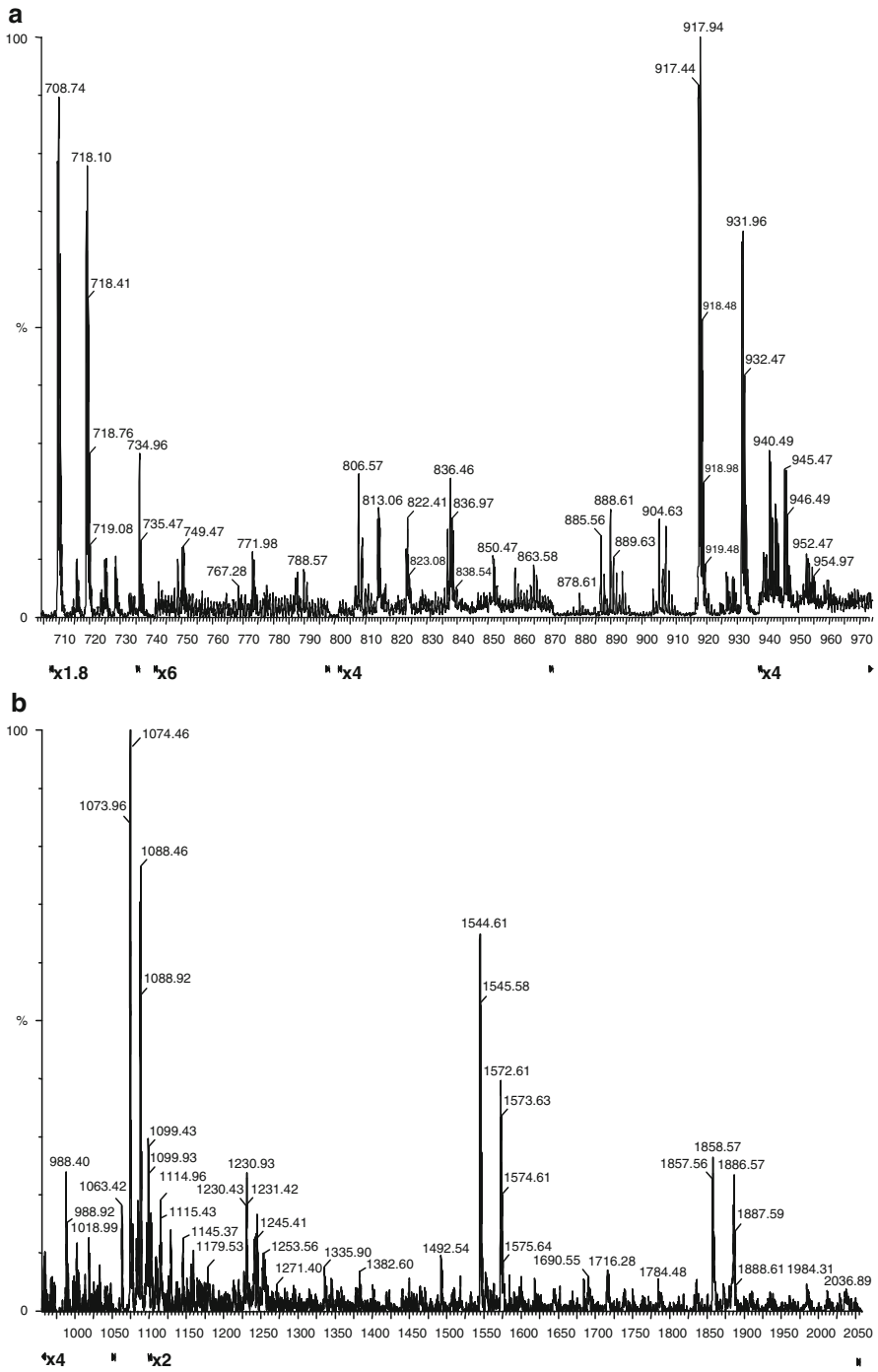

Fig. 8.4 Fully automated nanoESI chip QTOF MS in the negative ion mode of the ganglioside mixture extracted from the gray matter of adult cerebellum. Sample concentration: 5 pmol/μL in methanol. Acquisition time 3 min. Sampling cone potential 45–135 V. (**a**) *m/z* (700–980). (**b**) *m/z* (980–2,050) [88]

Table 8.1 Assignment of ganglioside components in the native mixture extracted from the gray matter of normal human adult cerebellum (male, 20 years) detected by nanoESI chip QTOF MS

Type of molecularion	*m/z* (monoisotopic) Detected	Calculated	Assigned structure
$[M+2Na-4H]^{2-}$	611.40	611.35	GM3 (d18:1/18:0)
$[M-H]^{-}$	1,179.57	1,179.74	
$[M-H]^{-}$	1,382.60	1,382.82	GM2 (d18:1/18:0)
$[M-2H]^{2-}$	734.96	734.91	GD3 (d18:1/18:0)
$[M+Na-2H]^{-}$	1,492.78	1,492.81	
$[M-2H]^{2-}$	748.99	748.93	GD3 (d18:1/20:0)
$[M-H]^{-}$	1,518.51	1,518.85	GM1, nLM1 and/or LM1 (d18:0/16:0)
$[M-2H]^{2-}$	771.98	771.93	GM1, nLM1 and/or LM1 (d18:1/18:0)
$[M-H]^{-}$	1,544.61	1,544.85	
$[M-2H]^{2-}$	786.00	785.92	GM1, nLM1 and/or LM1 (d18:1/20:0)
$[M-H]^{-}$	1,572.61	1,572.85	
$[M-H]^{-}$	1,690.55	1,690.93	Fuc-GM1 (d18:1/18:0)
$[M-H]^{-}$	1,716.56	1,716.94	Fuc-GM1 (d18:1/20:1)
$[M-2H]^{2-}$	836.46	836.45	GD2 (d18:1/18:0)
$[M-2H]^{2-}$	850.47	850.47	GD2 (d18:1/20:0)
$[M-2H]^{2-}$	917.44	917.48	GD1, nLD1 and/or LD1 (d18:1/18:0)
$[M+Na-3H]^{2-}$	928.45	928.47	
$[M-H]^{-}$	1,835.62	1,835.96	
$[M+Na-2H]^{-}$	1,857.56	1,857.95	
$[M-2H]^{2-}$	926.44	926.48	GD1, nLD1 and/or LD1 (t18:0/18:0)
$[M-2H]^{2-}$	924.44	924.49	GD1, nLD1 and/or LD1 (d18:1/19:0)
$[M-2H]^{2-}$	931.46	931.49	GD1, nLD1 and/or LD1 (d18:1/20:0)
$[M+Na-3H]^{2-}$	942.44	942.48	
$[M-H]^{-}$	1,885.60	1,885.98	
$[M-2H]^{2-}$	940.49	940.50	GD1, nLD1 and/or LD1 (t18:0/20:0)
$[M-2H]^{2-}$	938.44	938.50	GD1, nLD1 and/or LD1 (d18:1/21:0)
$[M-2H]^{2-}$	945.47	945.51	GD1, nLD1 and/or LD1 (d18:1/22:0)
$[M-2H]^{2-}$	954.46	954.51	GD1, nLD1 and/or LD1 (t18:0/22:0)
$[M-2H]^{2-}$	952.47	952.52	GD1, nLD1 and/or LD1 (d18:1/23:0)
$[M-2H]^{2-}$	958.46[a]	958.52	GD1, nLD1 and/or LD1 (d18:1/24:1)
$[M-2H]^{2-}$	966.44	966.53	GD1, nLD1 and/or LD1 (d18:1/25:0) or (d20:1/23:0)
$[M-2H]^{2-}$	988.40	988.49	Fuc-GD1 (d18:1/18:2)
$[M-2H]^{2-}$	990.40	990.51	Fuc-GD1 (d18:1/18:0)
$[M-2H]^{2-}$	999.41[a]	999.51	Fuc-GD1 (t18:0/18:0)
$[M-2H]^{2-}$	1,002.41	1,002.51	Fuc-GD1 (d18:1/20:2)
$[M-2H]^{2-}$	1,004.42	1,004.52	Fuc-GD1 (d18:1/20:0)
$[M-2H]^{2-}$	1,013.44[a]	1,013.53	Fuc-GD1 (t18:0/20:0)
$[M-2H]^{2-}$	1,018.99	1,019.02	GalNAc-GD1 (d18:1/18:0)
$[M-2H]^{2-}$	1,032.93[a]	1,033.03	GalNAc-GD1 (d18:1/20:0)
$[M-3H]^{3-}$	708.39	708.35	GT1 (d18:1/18:0)
$[M-2H]^{2-}$	1,062.96	1,063.03	
$[M+Na-3H]^{2-}$	1,073.92	1,074.02	
$[M+2Na-4H]^{2-}$	1,084.93	1,085.01	

(continued)

Table 8.1 (continued)

Type of molecularion	*m/z* (monoisotopic) Detected	Calculated	Assigned structure
$[M-3H]^{3-}$	714.41	714.35	GT1 (t18:0/18:0)
$[M+Na-3H]^{2-}$	1,082.92	1,083.02	
$[M-3H]^{3-}$	717.75	717.69	GT1 (d18:1/20:0)
$[M-2H]^{2-}$	1,076.97	1,077.04	
$[M+Na-3H]^{2-}$	1,087.95	1,088.03	
$[M+2Na-4H]^{2-}$	1,098.92	1,099.02	
$[M-3H]^{3-}$	723.75	723.70	GT1 (t18:0/20:0)
$[M+Na-3H]^{2-}$	1,096.93	1,097.04	
$[M+Na-3H]^{2-}$	1,094.95[a]	1,095.04	GT1 (d18:1/21:0)
$[M-3H]^{3-}$	727.11	727.04	GT1 (d18:1/22:0)
$[M+Na-3H]^{2-}$	1,101.92	1,102.05	
$[M+Na-3H]^{2-}$	1,108.92[a]	1,109.06	GT1 (d18:1/23:0)
$[M+Na-3H]^{2-}$	1,114.96	1,115.06	GT1 (d18:1/24:1)
$[M-3H]^{3-}$	722.39	722.35	*O*-Ac-GT1 (d18:1/18:0)
$[M-3H]^{3-}$	731.74	731.70	*O*-Ac-GT1 (d18:1/20:0)
$[M-2H]^{2-}$	1,128.95	1,129.05	Fuc-GT1 (d18:1/17:0)
$[M-2H]^{2-}$	1,144.89	1,145.06	Fuc-GT1 (t18:0/18:0)
$[M-2H]^{2-}$	1,159.89	1,159.08	Fuc-GT1 (t18:0/20:0)
$[M-3H]^{3-}$	805.40	805.38	GQ1 (d18:1/18:0)
$[M+Na-4H]^{3-}$	812.73	812.71	
$[M+2Na-4H]^{2-}$	1,230.43	1,230.56	
$[M+3Na-5H]^{2-}$	1,241.43	1,241.55	
$[M-3H]^{3-}$	814.74	814.72	GQ1 (d18:1/20:0)
$[M+Na-4H]^{3-}$	822.07	822.05	
$[M+2Na-4H]^{2-}$	1,244.42	1,244.57	
$[M-3H]^{3-}$	819.38[a]	819.38	*O*-Ac-GQ1 (d18:1/18:0)
$[M+Na-4H]^{3-}$	826.73[a]	826.71	

Reprinted with permission from [88]
d dihydroxy sphingoid base, *t* trihydroxy sphingoid base
[a]Low intensity ions

later developmental phase. Therefore, based on the MS data it was hypothesized that these modifications of cerebellum gangliosides start to reach a relevant level only later, during extrauterine brain development and maturation. By combining in high-throughput mode fully automated nanoESI chip MS infusion with CID MS^2 at variable RF signal amplitudes, a complete structural characterization of two cerebellum-associated ganglioside species, GD1 (d18:1/20:0) and GM2 (d18:1/19:0), was accomplished in only 1 minute of signal acquisition for each MS^2 experiment and with a sample consumption, situated in the femtomole range.

8.3.3 Defined Cerebrum Regions

8.3.3.1 Hippocampus

Hippocampus is a brain region situated inside the temporal lobe, under the cerebral cortex. This particular sector of the brain belongs to the limbic system and plays a vital role in learning, memory formation, and orientation [45]. Hippocampus is one of the first brain areas displaying the neurodegenerative pathology in Alzheimer's disease (AD). Consequently, the primary clinical symptoms of AD are due to the impairment of hippocampus functions and are characterized by disorientation and progressive loss of memory. From this perspective, the evaluation of ganglioside expression in this brain region has a particular clinical relevance for early detection of alteration that is attributable to Alzheimer's disease [55].

Mass spectrometry was introduced in human hippocampus ganglioside analysis in 2006 via an analytical platform encompassing fully automated chip-base nano-ESI on a NanoMate robot coupled to a high-resolution hybrid QTOF instrument [82]. Comparative analysis of gangliosides in fetal of different gestational weeks vs. adult hippocampus revealed a specific expression and structure of individual species, which depend on the brain development stage. Hence, polysialylated structures were found markers of the earlier fetal developmental stage. Trisialylated species were found better expressed in fetal hippocampus of 15 (FH15) and 17 (FH17) gestational weeks, while tetrasialylated components, in particular GQ1 forms, were found associated to FH15 (Fig. 8.5, Table 8.2) and not at all to FH17 and adult hippocampus of 20 years of age (AH20). Remarkably, tandem MS carried out using CID at low ion acceleration energies provided data consistent with GQ1b isomer in F15 hippocampus.

In contrast with sialylation, Fuc or GalNAc modifications of the ganglioside chain were found associated to the tissue in its either later fetal development stage or adulthood; fucosylated components were identified in FH17 (Fuc-GD1) and AH20 (Fuc-GD1 and Fuc-GT1) but not observed in FH15, while a GalNAc-GD1 species was found only in AH20. Actually, in this study using nanoESI chip MS characterized by high ionization efficient, sensitivity, and reproducibility, the topo-specific pattern and development-induced ganglioside modifications were for the first time reliably demonstrated and correlated with the biological expectations.

8.3.3.2 Caudate Nucleus

Caudate nucleus (*nucleus caudatus*, NC) is an essential part of the brain learning and memory system located within the basal ganglia of the brain of many animal species. Other functions which may be associated with this part of the brain include voluntary motor control and a regulating role in controlling the threshold potential

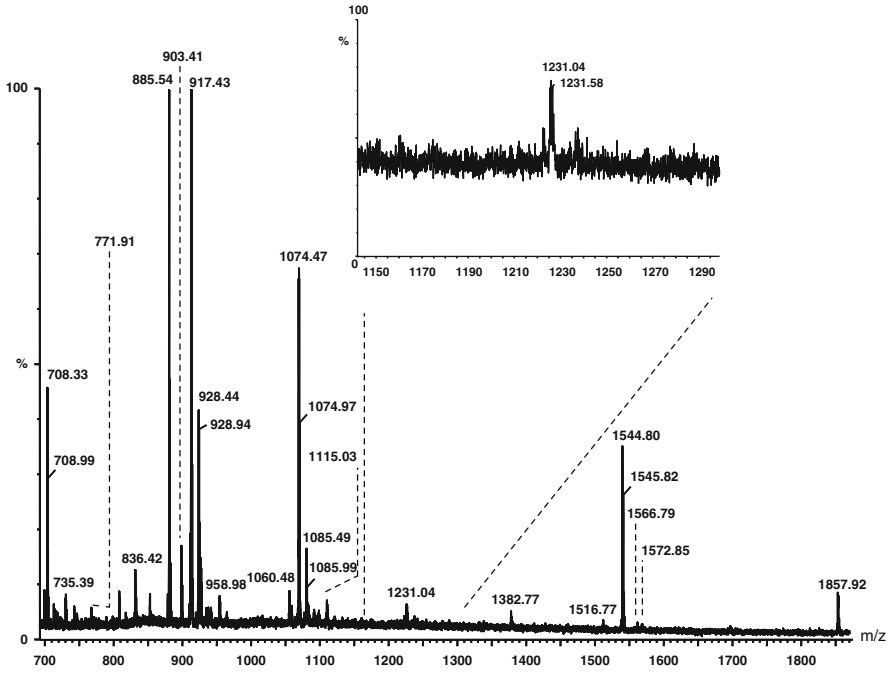

Fig. 8.5 NanoESI chip QTOF MS in the negative ion mode of the FH15 ganglioside mixture. ESI voltage 1.80 kV; cone voltage 40–100 V; Solvent MeOH. Sample concentration 3 pmol/μL; Inset: expanded area *m/z* (1,150–1,300). Reprinted with permission from Vukelić et al. [82]

Table 8.2 Comparative assignment of the ganglioside species identified by negative ion mode nanoESI chip QTOF MS in fetal and adult hippocampus

	m/z (monoisotopic)					
Proposed structure	Experimental	Theoretical	Molecular ion	FH15	FH17	AH20
GM3(d18:1/16:0)	1,151.94	1,151.71	$[M-H]^-$	+	–	–
GM2(d18:1/18:0)	1,382.77	1,382.82	$[M-H]^-$	+	+	+
GM1(d18:1/18:0)	771.91	771.93	$[M-2H]^{2-}$	+	+	+
	1,544.80	1,544.85	$[M-H]^-$			
	1,566.79	1,566.83	$[M+Na-2H]^-$			
GM1(d18:1/20:0)	786.05	785.92	$[M-2H]^{2-}$	+	+	+
	1,572.85	1,572.85	$[M-H]^-$			
GD3(d18:1/18:0)	734.88	734.91	$[M-2H]^{2-}$	+	+	+
GD2(d18:1/18:0)	836.42	836.45	$[M-2H]^{2-}$	+	+	+
GD1(d18:1/16:0)	903.41	903.46	$[M-2H]^{2-}$	+	+	–
GD1(d18:1/18:0)	917.43	917.48	$[M-2H]^{2-}$	+	+	+
	928.44	928.47	$[M+Na-3H]^{2-}$			
	1,857.92	1,857.95	$[M+Na-2H]^-$			
	1,879.94	1,879.93	$[M+2Na-3H]^-$			

(continued)

Table 8.2 (continued)

Proposed structure	*m/z* (monoisotopic)		Molecular ion	FH15	FH17	AH20
	Experimental	Theoretical				
GD1(d18:1/20:0)	931.44	931.49	$[M-2H]^{2-}$	+	+	+
	942.39	942.48	$[M+Na-3H]^{2-}$			
GD1(d18:1/24:1)	958.98	958.52	$[M-2H]^{2-}$	+	+	+
Fuc-GD1(t18:0/18:0)	999.47	999.51	$[M-2H]^{2-}$	–	+	+
Fuc-GD1(t18:0/20:0)	1,013.89	1,013.53	$[M-2H]^{2-}$	–	–	+
GalNAc-GD1(d18:1/18:0)	1,018.91	1,019.02	$[M-2H]^{2-}$	–	–	+
GT1(d18:1/18:1)	1,060.48	1,061.03	$[M-2H]^{2-}$	+	–	–
GT1(d18:1/18:0)	708.33	708.35	$[M-3H]^{3-}$	+	+	+
	1,074.47	1,074.02	$[M+Na-3H]^{2-}$			
	1,085.49	1,085.01	$[M+2Na-4H]^{2-}$			
GT1(d18:1/20:0)	717.91	717.69	$[M-3H]^{3-}$	+	+	+
	1,088.39	1,088.03	$[M+Na-3H]^{2-}$			
	1,099.40	1,099.02	$[M+2Na-4H]^{2-}$			
GT1(d18:1/24:1)	1,115.03	1,115.06	$[M+Na-3H]^{2-}$	+	+	+
Fuc- GT1(d18:1/17:0)	1,129.40	1,129.05	$[M-2H]^{2-}$	–	–	+
GQ1(d18:1/18:0)	1,231.04	1,230.56	$[M+2Na-4H]^{2-}$	+	–	–
	1,241.81	1,241.55	$[M+3Na-5H]^{2-}$			

Reprinted with permission from Vukelic et al. [81]
+ the structure was detected; – the structure was not detected

for general neuron activation and thereby preventing overload through positive feedback loops [21, 54]. Various disorders such as depression, Huntington's disease, Parkinson's disease, attention deficit disorder, schizophrenia, and obsessive compulsive disorder are strongly related with this part of the brain [6, 79, 86]. From this perspective, certainly, the evaluation of ganglioside expression in this brain region is essential for neurological studies. The literature data related to NC glycolipid investigation using other methods than MS is limited to a report on a few identified species. The first consistent compositional and structural analysis of gangliosides extracted from adult human NC was carried out using tandem mass spectrometry on a high-capacity ion trap (HCT) instrument equipped with nanoESI chip in the negative ion mode [65]. Over 80 components differing in the carbohydrate chain and ceramide composition, with a large range of fatty acids, were for the first time discovered in NC. NC was found dominated by mono-, di-, and trisialylated ganglioside structures. Twenty-two species were found to contain one sialic acid (Neu5Ac) moiety, 28 species disialylated, and 20 trisialylated. MS analysis revealed that the carbohydrate chains of gangliosides in human NC vary from one to four monosaccharide units, while the Cer moiety exhibits a high heterogeneity in the fatty acid and/or sphingoid base composition. Also, four tetrasialylated and two pentasialylated structures, i.e., a GP3 (d18:1/12:0) and a GP2 (d18:1/20:0), were detected and identified in the NC extract. The incidence of species with such a high sialylation grade in other adult brain areas was not reported before. Therefore, the identification in the NC of these structures has a particular biological and biochemical value. Besides, MS screening provided information on the incidence in NC of

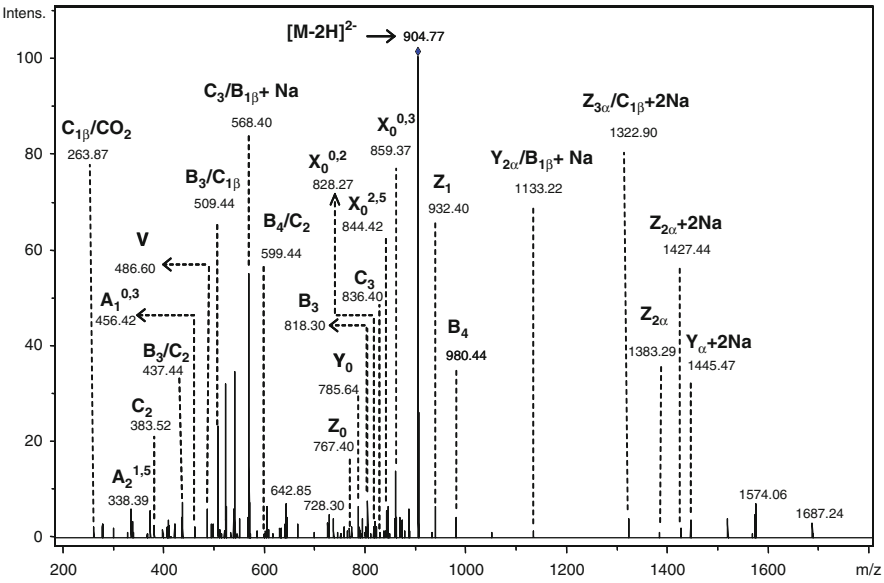

Fig. 8.6 NanoESI chip HCT CID MS^2 of the $[M+2Na-4H]^{2-}$ at *m/z* 904.77 corresponding to GM1 (d18:1/34:2) ganglioside species detected in adult human NC. Solvent: MeOH. Sample concentration: 3 pmol/μL. Acquisition time: 1.5 min. Chip ESI −0.85 kV; capillary exit −30 V. The assignment of the fragment ions is according to the nomenclature [14]. Reprinted with permission from Serb et al. [65]

several glycoforms modified by *O*-Fuc and *O*-Ac attachments and/or lactonization. In addition to these findings, as no less than 14 species with fatty acids chains exceeding 30 carbon atoms were discovered in NC, the presence of unusually long fatty acid chains in Cer composition is another feature, which distinguishes fundamentally NC from the other brain regions. In the second stage of NC ganglioside research by MS, a NC-associated structure exhibiting a rare ceramide composition with 34 carbon atoms in the fatty acid chain was fragmented by CID MS^2 (Fig. 8.6). Adequate fragmentation conditions induced the formation of parent ions diagnostic not only for the carbohydrate sequence but also for the highly specific and at the same time unusual fatty acid chain within the lipid part. Hence, the spectrum in Fig. 8.6 and the derived fragmentation scheme in Fig. 8.7 show that the fatty acid chain consisting of 34 carbon atoms bearing two double bounds is very well documented by the V-type fragment ion.

8.3.3.3 Sensory and Motor Cortex

Sensory cortex (SC) is a brain region located on the lateral postcentral gyrus of the parietal lobe and represents the main sensory receptive area. Damages of this region might affect the ability to recognize objects and, in an extreme condition, induce impairment in the contra-lateral side perception of the subject outer environment [11].

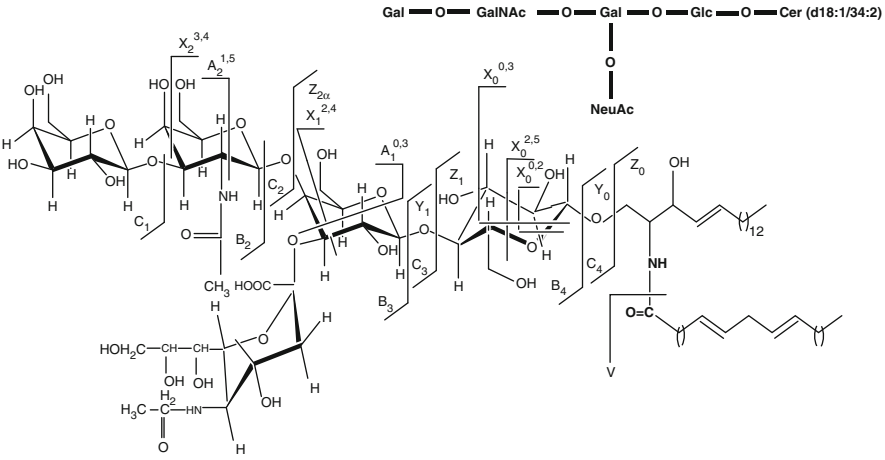

Fig. 8.7 Fragmentation scheme of the $[M+2Na-4H]^{2-}$ ion at *m/z* 904.77 corresponding to GM1 (d18:1/34:2) ganglioside species detected in adult human NC. Reprinted with permission from Serb et al. [65]

Motor cortex (MC) represents an area of the cerebral cortex responsible for the planning, control, and completing voluntary movements [12]. MC is the main contributor to generating neural impulses, which pass down to the spinal cord and control the execution of movements. Injury of this brain area creates spastic contralateral weakness, which is most prominent in the distal extremities [12].

Being situated in close proximity, MC and SC are often both affected by various disorders and accidents such as cerebral vascular accident, amyotrophic lateral sclerosis (ALS), multiple sclerosis, Ramsay Hunt syndrome, Parkinson disease (PD) and brain cancer [4, 34, 48]. Lately, positron emission tomography-PET [50], and functional magnetic resonance imaging-fMRI [10] emerged as highly efficient imaging techniques for the study of functional reorganization of MC and SC.

Several studies demonstrated that use of GM1 ganglioside resulted in significant symptom reduction in Parkinson's disease (PD) patients [63]. Also, marked aberrations in brain ganglioside profiles detected in MC were found related to ALS [76].

The actual trends in the management of MC and SC afflictions are oriented towards a combination of imaging methods for diagnostic and development of novel and effective drugs for treatment. In this regard, the last findings indicate that gangliosides are in the focus of research as possible bases for vaccines and drug therapies-oriented medication.

In a recent study high-resolution tandem MS on a QTOF instrument was developed and for the first time applied for the assessment of ganglioside composition and structure in specimens of human MC and SC [18]. Screening of the MC and SC extracts in the negative ion mode nanoESI, under identical conditions, disclosed the presence of 90 distinct gangliosides in both native mixtures, of which 48 in MC and 42 in SC. Remarkably, in MC, 2 tetra-, 11 tri-, and 20 disialylated ganglioside components were discovered in contrast with SC where only 8 tri- and 13 disialylated

molecules were detected. Of high importance is the identification in MC of tetrasialylated GQ1(d18:1/18:0) and GQ1(d18:1/20:0) species which were not observed in SC. MC mixture was also found to contain a higher number of fucosylated and acetylated species as well as gangliosides with trihydroxylated sphingoid bases. These findings demonstrated that the sialylation degree, fucosylation and acetylation pattern, and sphingoid base hydroxylation of the gangliosides expressed in the two cortex regions are to be correlated with the specific functions of MC and SC.

CID at low ion acceleration energies applied to elucidate the structure of fucosylated species Fuc-GM1 (d18:1/20:0) revealed the presence in MC of an isomer exhibiting both Neu5Ac and Fuc residues linked at the inner galactose. Since this structure was not reported previously, seemingly Fuc-GM1 (d18:1/20:0) species with sialylated and fucosylated inner galactose is associated to the motor cortex.

8.3.3.4 Neocortex

Neocortex is the newest area in brain development of mammals [29, 38]. In humans it accounts for about 76 % of the brain volume, as the outer layer of the cerebral hemispheres, made up of six layers. Among mammals human neocortex is the largest [31], allowing a new level of advanced behavior such as particular social behavior, language, and high-level consciousness. Neocortex is involved also in other elevated functions such as sensory perception, generation of motor commands, spatial reasoning, and all of the conscious thoughts. Basically, the neocortex enables the most complex mental activity, which is associated with humans.

Gangliosides extracted from fetal neocortex of 36 gestational weeks were analyzed by mass spectrometry using a HCT with nanaelectrospray chip-based infusion on a NanoMate robot [17]. Eighty-nine ganglioside species differing in their carbohydrate chain structure and ceramide composition were identified in the neocortex within only 2 min of signal acquisition for single MS screening experiments. A notable characteristic is the identification in neocortex of six GQ species and also asialo- components having the oligosaccharide composition $HexNAcHex_2$ and $HexHexNAcHex_2$.

Ganglioside chains decorated with peripheral attachments such as Fuc and/or *O*-Ac were previously reported as associated to the tissue in its advanced developmental phase. Indeed, MS investigation of neocortex provided relevant data documenting 12 fucosylated species, of which three GT1, two GT2, two GD2, two GM4, one GT3, one GD1 and one GA2, seven *O*-acetylated structures corresponding to GM1, GD3, GD1, GT1, and GQ1, exhibiting high heterogeneity in their ceramide motifs. Contrastingly, in other fetal brain regions a much lower number of *O*-acetylated species and no species modified by fucosylation were found. This particular aspect suggests that Fuc- and *O*-Ac- gangliosides are rather associated with the neocortex as the most recently developed human brain region, where the high level of thinking takes place and specialized integrative tasks are processed. The large number of ganglioside species identified in neocortex is to be correlated with the complexity of the functions coordinated by this region and with its central role in the higher mental functions as language, memory, thinking,

attention, abstraction, and perception in humans. The results obtained in direct comparative MS analyses of neocortex vs. brain lobes [17] have also shown that differences in ganglioside expression in fetal human brain are dependent rather on the phylogenetic development than topographic factors. This feature, discovered exclusively by MS, provides a novel insight into the major role of gangliosides in human brain evolution and advancement of its functions in comparison with the other mammals.

8.4 Gangliosides in Pathological Brain

8.4.1 Neurodegenerative Diseases

Neurodegenerative diseases represent a group of ailments characterized by the deterioration of the structure or function of neurons up to the death of neurons. Neurodegenerative diseases including Parkinson's, Alzheimer's, Huntington's diseases, ALS, anencephaly, spinocerebellar ataxia, and dementia arise as a consequence of neurodegenerative processes taking place from molecular to systemic level.

Gangliosides trigger a variety of neurodegenerative diseases [63, 64] from autoimmune-induced neuropathies caused by anti-ganglioside auto-antibodies to lipidoses, a group of inherited metabolic disorders caused by the accumulation of gangliosides in cell bodies due to a obstruction of their catabolic pathways [59].

Gangliosides were also shown to have neuritogenic and neuronotrophic activity [8] and to facilitate repair of neuronal tissue after mechanical, biochemical, or toxic injuries. In AD administration of GM1, having a high affinity for Aβ resulted in the reduction of Aβ level in the brain, suggesting that GM1 might serve as the therapeutic agent reducing/preventing brain amyloidosis by sequestering the plasma Aβ [3]. On the other hand, interactions of Aβ (1–40) with ganglioside-containing membranes, particularly with membrane rafts enriched in GM1 and GM3, were hypothesized to be involved in the pathogenesis of AD [52]. Using conventional high-performance thin-layer chromatographic separation/detection, immunochemical, and immunohistochemical detection methods, specific changes in ganglioside expression and quantity in investigated human brain regions in AD disease were discovered [32, 35].

MALDI TOF MS in combination with a method for transferring lipids separated on a TLC-plate to a poly-vinylidene difluoride membrane and direct mass spectrometric analysis of the individual lipids on the membrane was applied to the analysis of individual lipids and ganglioside molecular species in neural diseases [78]. In the case of Alzheimer's disease the expression of GD1b and GT1b gangliosides was found diminished in the hippocampal gray matter than in the hippocampal gray matter of patients with Parkinson's disease or the control patients [72]. The analysis of single ganglioside molecular species in patients with Alzheimer's disease demonstrated a major decrease of species exhibiting (20:1/18:0) ceramide composition.

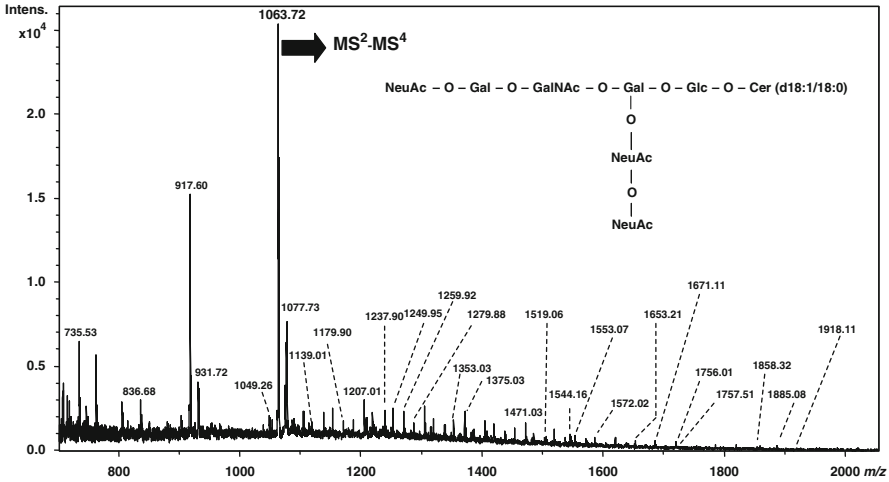

Fig. 8.8 NanoESI chip HCT MS in negative ion mode of native ganglioside mixture from glial islands of anencephalic fetus. Solvent MeOH. Sample concentration 5 pmol/μL. Acquisition time 7 min. Chip ESI −0.8 kV; capillary exit −50 V. Reprinted with permission from Almeida et al. [1]

These results imply that Alzheimer's disease is a ganglioside metabolic disease affecting the hippocampal area. Such findings explain in part the major symptoms of the disease, which are related to abilities promoted by hippocampus.

In anencephaly, a congenital malformation of the fetal brain occurring when the cephalic end of the neural tube fails to close [7], the first assessment of ganglioside composition by MS was reported in 2001 [80]. In this study nanoESI QTOF MS and tandem MS were applied for the first time for compositional and structural identification of native gangliosides from anencephalic cerebral residue. By this approach it was found that the total ganglioside concentrations in the anencephalic cerebral remnant and in cerebellum were significantly lower than in the corresponding regions of the age-matched brain used as control. In the cerebral remnant, GD3, GM2 and GT1b, GM1b nLM1, and nLD1 were found highly expressed. Oppositely, GD1a was found better expressed in the anencephalic cerebellum, while GQ1b was reduced in both anencephalic regions. In agreement with previously acquired information using immunochemical methods, by nanoESI MS, members of the neolactoseries gangliosides were also discovered in anencephalic brain tissues.

Supplementary information supporting a major modification of ganglioside expression in anencephalic vs. age-matched normal brain tissue were collected by a superior methodology based on fully automated nanoESI chip MS and multistage MS using the coupling of NanoMate robot to HCT MS tuned in the negative ion mode [1]. The ganglioside mixture extracted from glial islands of fetal anencephalic brain tissue was investigated in comparison with the gangliosides from a normal fetal frontal lobe. Under identical instrumental and solution conditions, 25 distinct species in the mixture from anencephalic tissue (Fig. 8.8, Table 8.3) vs. 44 of

Table 8.3 Assignment of the major ions detected by negative ion mode nanoESI chip HCT MS in the ganglioside mixture extracted from the glial islands of anencephalic fetus

m/z monoisotopic	Molecular ion	Proposed structure
735.12	$[M-2H]^{2-}$	GD3(d18:0/18:0)
836.71	$[M-2H]^{2-}$	GD2(d18:1/18:0)
851.60	$[M-H]^{-}$	GD2(d18:1/20:0)
918.08	$[M-2H]^{2-}$	GD1(d18:1/18:0)
931.72	$[M-2H]^{2-}$	GD1(18:1/20:0)
952.80	$[M-H]^{-}$	GD1(d18:1/23:0)
1,037.60	$[M-H]^{-}$	$HexNAcHex_2Cer$ (d18:0/14:0) or (d16:0/16:0)
1,041.60	$[M-H]^{-}$	GM4 (d18:1/20:2)
1,049.18	$[M-2H]^{2-}$	GT1(18:1/16:0)
1,063.33	$[M-2H]^{2-}$	GT1(d18:1/18:0)
1,065.63	$[M-H]^{-}$	$HexNAcHex_2Cer$ (d18:0/16:0)
1,077.71	$[M-2H]^{2-}$	GT1(d18:1/20:0)
1,104.78	$[M-2H]^{2-}$	GT1(d18:1/24:0)
1,139.01	$[M-H]^{-}$	GM3(d18:1/14:0) or (d18:1/h14:0) or $HexNAcHex_2Cer$ (d18:1/22:4)
1,151.71	$[M-H]^{-}$	GM3 (d18:1/16:0)
1,165.80	$[M-H]^{-}$	$HexNAcHex_2Cer$ (t18:0/22:0) or (d18:0/h22:0) or (d18:2/24:4)
1,167.82	$[M-H]^{-}$	GM3 (t18:1/16:0) or (d18:1/h16:0) or $HexNAcHex_2Cer$ (d18:1/24:4)
1,179.74	$[M-H]^{-}$	GM3 (d18:1/18:0)
1,181.75	$[M-H]^{-}$	GM3 (d18:0/18:0)
1,206.77	$[M-H]^{-}$	GM3(d18:1/20:0)
1,221.33	$[M-H]^{-}$	GM3(d18:1/18:0)
1,235.81	$[M-H]^{-}$	GM3 (d18:1/22:0)
1,237.81	$[M-H]^{-}$	GM3 (d18:0/22:0)
1,249.78	$[M-H]^{-}$	*O*-Ac-GM3 (d18:1/20:0) (or GM3 (18:1/23:0)
1,253.02	$[M-H]^{-}$	$HexHexNAcHex_2Cer$(d18:1/18:0)
1,259.79	$[M-H]^{-}$	GM3 (d18:1/24:2)
1,261.81	$[M-H]^{-}$	GM3 (d18:1/24:1)
1,263.83	$[M-H]^{-}$	GM3 (d18:1/24:0)
1,265.84	$[M-H]^{-}$	GM3 (d18:0/24:0)
1,275.80	$[M-H]^{-}$	*O*-Ac-GM3 (d18:1/22:1) (or GM3 (20:1/23:1)
1,277.80	$[M-H]^{-}$	*O*-Ac-GM3 (d18:1/22:0) (or GM3 (20:1/23:0)
1,279.81	$[M-H]^{-}$	*O*-Ac-GM3 (d18:0/22:0) (or GM3 (20:0/23:0)
1,301.82	$[M-H]^{-}$	*O*-Ac-GM3 (d18:1/24:2)
1,353.03	$[M-H]^{-}$	GM2 (d18:1/16:0)
1,354.79	$[M-H]^{-}$	GM2 (d18:1/16:0)
1,383.21	$[M-H]^{-}$	GM2 (d18:1/18:0)
1,384.81	$[M-H]^{-}$	GM2 (d18:0/18:0)
1,437.01	$[M-H]^{-}$	GM2 (d18:1/22:0)
1,442.78	$[M-H]^{-}$	GD3 (d18:1/16:0)
1,444.80	$[M-H]^{-}$	GD3 (d18:0/16:0)
1,468.79	$[M-H]^{-}$	GD3 (d18:1/18:1)

(continued)

Table 8.3 (continued)

m/z monoisotopic	Molecular ion	Proposed structure
1,471.03	$[M-H]^-$	GD3(d18:1/18:0)
1,472.83	$[M-H]^-$	GD3 (d18:0/18:0)
1,519.10	$[M-H]^-$	GM1, nLM1 and/or LM1 (d18:0/16:0)
1,544.16	$[M-H]^-$	GM1, nLM1 and/or LM1 (d18:1/18:0)
1,545.20	$[M-H]^-$	GM1, nLM1 and/or LM1 (d18:1/18:0)
1,805.23	$[M-H]^-$	GT3(d18:1/18:0)
1,836.40	$[M-H]^-$	GD1(d18:1/18:0)

Reprinted with permission from [1]

which 4 asialylated in the normal frontal lobe were for the first time identified. These results indicate that a high number of ganglioside species associated to anencephaly could be ionized and discriminated only by employing chip-based electrospray. Interestingly, GD3 (d18:1/18:0), GD2 (d18:1/18:0), GM1 (d18:1/18:0), and their neolacto or lacto-series isomers were detected as ions of similar low abundances in both mixtures, while GT1 (d18:1/18:0) and GD1 (d18:1/18:0) were found highly expressed in ancencephalic brain tissue (Table 8.4). Moreover, several structures such as GT1, GQ1, and GQ2 emerged clearly associated to anencephaly. This prominent occurrence of polysialylated structures in anencephaly is basically an effect to be used for the diagnosis of the brain development stagnation, characteristic to this disease [1]. In view of the results obtained by MS/MS, the earlier report [80] has postulated that GT1b is one of the disease markers; however, because of the limited information obtained by fragmentation analysis in a single CID stage, validation of sialylation sites could not be accomplished. To close this gap, a nanoESI chip CID MS^n protocol [1] for fine investigation of the anencephaly-specific GT1 (d18:1/18:0) species was elaborated (Fig. 8.9a–d). The beneficial combination of chip infusion, high capacity of ion storage, and multistage sequencing rendered ions diagnostic for the disialo ($Neu5Ac_2$) element localization at internal galactose moiety. Hence, chip MS results disclosed for the first time GT1b species in the cerebral remnant of anencephalic brain.

8.4.2 Primary Brain Tumors

Primary brain tumors account for approximately 2 % of all adult malignancies and are responsible for about 7 % of years of life lost prior to age 70. In childhood, 20 % of all malignancies identified prior to 15 years of age are primary brain tumors. This situates the primary brain tumors on the second place among the most frequent type of cancer identified in children. For primary brain tumors therapy, drastic surgical resection radiation and chemotherapy are especially applied [43]. These methods are frequently problematic firstly because of collateral brain tissue sensitivity to disruption and secondly because of the toxicity accompanied by side effects of the therapeutic agents.

Table 8.4 Comparative overview upon gangliosides and asialo-gangliosides detected by negative ion mode nanoESI chip HCT MS in the glial islands of anencephalic fetus and in the frontal lobe of healthy fetal brain

Ganglioside species	Proposed structure	Anecephaly	Normal frontal lobe
GM1	nLM1 and/or LM1 (d18:0/16:0)	+	+
	nLM1 and/or LM1 (d18:1/18:0)	+	+
	nLM1 and/or LM1 (d18:0/20:0)	+	−
	(d18:1/16:0)	+	+
	(d18:1/18:0)	−	+
	(d18:1/22:0)	−	+
GM3	(d18:1/14:0) or (d18:1/h14:0) or $HexNAcHex_2Cer$ (d18:1/22:4)	+	+
	(d18:1/16:0)	−	+
	(t18:1/16:0) or (d18:1/h16:0) or $HexNAcHex_2Cer$(d18:1/24:4)	−	+
	(d18:1/18:0)	+	+
	(d18:0/18:0)	−	+
	(d18:1/20:0)	+	+
	(d18:1/22:0)	−	+
	(d18:0/22:0)	+	+
	(d18:1/24:2)	+	+
	(d18:0/24:0)	+	+
	(d18:1/24:1)	−	+
	(d18:1/24:0)	−	+
	O-Ac-GM3 (d18:1/20:0) or GM3 (18:1/23:0)	−	+
	O-Ac-GM3 (d18:1/22:1) or GM3 (20:1/23:1)	−	+
	O-Ac-GM3 (d18:1/22:0) (or GM3 (20:1/23:0)	−	+
	O-Ac-GM3 (d18:0/22:0) (or GM3 (20:0/23:0)	+	+
	O-Ac-GM3 (d18:1/24:2)	−	+
GM4	(d18:1/20:2)	−	+
GD1	(d18:1/18:0)	+	+
	(d18:1/20:0)	+	+
	(d18:1/23:0)	−	+
	(d18:1/24:1)	+	−
	(d18:0/18:0)	+	−
GD2	(d18:1/18:0)	+	+
	(d18:1/18:1)	+	−
	(d18:1/24:1)	+	−
	(d18:1/24:0)	+	−
	(d18:1/20:0)	−	+
GD3	(d18:0/18:0)	+	+
	(d18:1/16:0)	−	+
	(d18:0/16:0)	−	+
	(d18:1/18:1)	−	+
	(d18:1/18:0)	+	+
	(d18:1/24:1)	+	−

(continued)

Table 8.4 (continued)

Ganglioside species	Proposed structure	Anecephaly	Normal frontal lobe
GT1	(18:1/16:0)	+	+
	(d18:1/18:0)	+	+
	(d18:0/20:0)	+	−
	(d18:1/20:0)	+	+
	(d18:1/24:0)	−	+
GT3	(d18:1/18:0)	−	+
	(d18:1/24:0)	−	+
	(d18:1/24:1)	+	−
GQ1	(d18:1/18:0)	+	−
Asialo-species	$HexNAcHex_2Cer$ (d18:0/14:0) or (d16:0/16:0)	−	+
	$HexNAcHex_2Cer$ (d18:0/16:0)	−	+
	$HexNAcHex_2Cer$ (t18:0/22:0) or (d18:0/h22:0) or (d18:2/24:4)	−	+
	$HexHexNAcHex_2Cer$ (d18:1/18:0)	−	+

Reprinted with permission from [1]

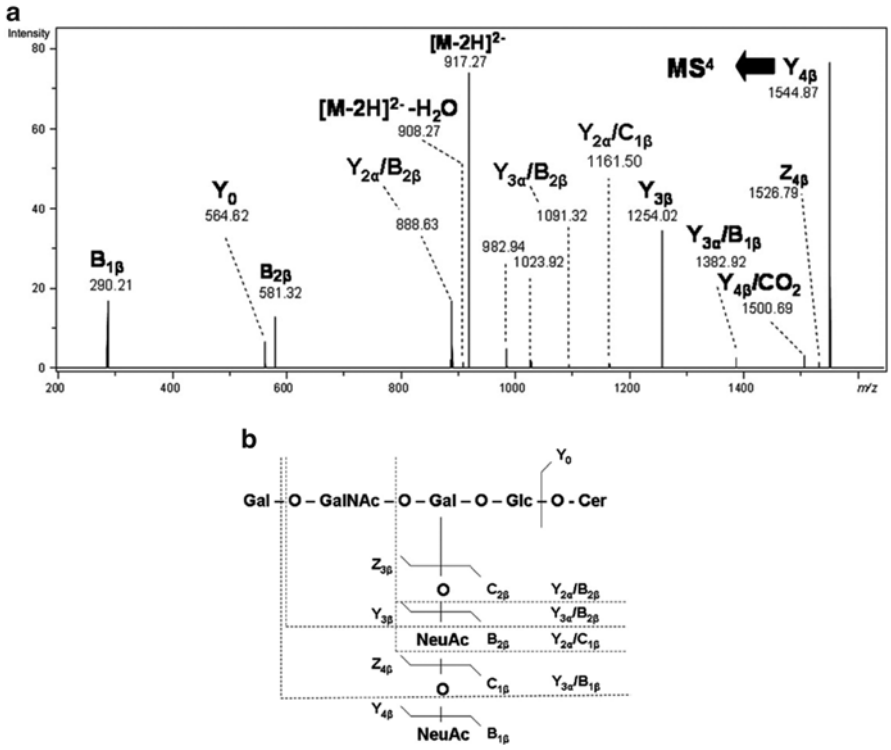

Fig. 8.9 NanoESI chip HCT multistage MS of the doubly charged ion at *m*/*z* 1,063.34 corresponding to GT1 (d18:1/18:0) species from glial islands of anencephalic fetus mixture: (**a**) MS^3. (**b**) fragmentation scheme of ion at *m*/*z* 917.32. (**c**) MS^4. (**d**) fragmentation scheme of the ion at *m*/*z* 1,544.87. The assignment of the fragment ions is according to the nomenclature [14]. Reprinted with permission from Almeida et al. [1]

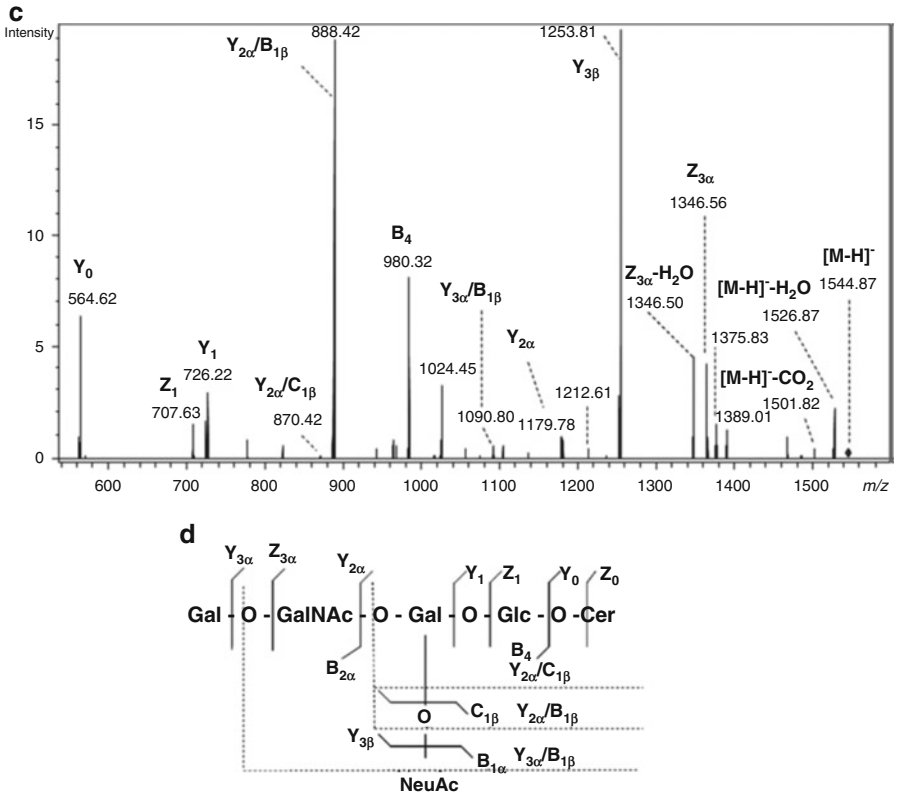

Fig. 8.9 (continued)

Tumorigenesis/malignant transformation is accompanied by aberrant cell surface composition, particularly due to irregularities in glycoconjugate glycosylation pathways. Various glycosyl epitopes constitute tumor-associated antigens [47, 73]. Some of them promote invasion/metastases, while some other suppress tumor progression. Among molecules bearing characteristic glycosyl epitopes causing such effects are also gangliosides. Gangliosides were recently shown to play an important role in brain tumor development, progression, and treatment [5, 37, 46, 66].

Glycosphingolipid-dependent cross-talk between glycosynapses interfacing tumor cells with their host cells has been even recognized as a basis to define tumor malignancy [23]. Specific changes of gangliosides pattern in brain tumors correlating with tumor histopathological origin, malignancy grade, invasiveness, and progression have been observed [67, 74]. Tumor cells of neuroectodermal origin may shed their gangliosides into circulation, resulting in higher ganglioside concentrations in serum [16]. This shedding of gangliosides into interstitial spaces and blood of oncological patients has been suggested to be involved in increased tumor cell growth and lack of immune cell recognition. Although higher concentrations of serum gangliosides in oncological patients comparing to healthy individuals have been reported [60], there have been no data on comparison of ganglioside

concentrations in serum or cerebrospinal fluid before and after surgical removal of tumor in individual patients. Glycoantigens and lipoantigens have been recognized as relevant and potentially valuable diagnostic and prognostic markers and tumor molecular targets for development/production of specific antitumor drugs [41] such as glycolipids-based vaccines, but their investigation in this regard has been neglected comparing to proteins.

Except for mass spectrometry, several biophysical and biochemical methods such as Raman spectroscopy, immunocytochemistry, flow cytometry, western blotting, transwell assays, and mid-infrared spectromicroscopy were developed and optimized for the determination of lipid/glycolipid molecular markers in brain tumors [17, 36, 69, 70]. Nevertheless, a large number of low abundant tumor-associated species could not be detected by these approaches. Using these methods, the data acquired on ganglioside composition in human brain tumors, sera and cerebrospinal fluid were restricted to several major species; many less abundant species have not been structurally characterized. This emphasized a need for detailed and systematic screening and structural characterization of brain tumor glycoconjugate composition, which could adequately be achieved only combining up-to-date, ultrasensitive, high-resolution methodological approaches of detection and sequencing of biomolecules, such as advanced mass spectrometry combined with bioinformatics for data interpretation.

8.4.2.1 Benign Tumors

Meningioma

Meningiomas are a group of tumors of the meninges, the membranes surrounding the brain and spinal cord. Meningiomas occur from the arachnoid cap cells, which enclose and adhere to the dura mater.

According to WHO [42] meningiomas are classified as benign (WHO grade I), atypical (WHO grade II), and malignant/anaplastic (WHO grade III). Ninety percent of all diagnosed meningiomas are benign. Due to the reduced incidence of the malignant type, in general meningiomas are regarded as tumors treatable by surgery [24]. Altogether, meningiomas represent about 13–30 % of the primary intracranial neoplasms, being among brain tumors only less frequent than gliomas.

If low-grade meningiomas are treated by surgical resection, which yields permanent healing, higher grade forms require radiation therapy following tumor removal [85]. Meningiomas can usually be surgically resected only if the tumor is superficial on the dural surface and accessible; if invasion of the adjacent bone/tissue already occurred, total removal is not feasible and the treatment is impeded. This particular aspect, which applies to tumors in their latter form, together with the discrepancy between the biological behavior and tumor grade opened lately new research directions in bioanalytics and molecular medicine towards discovery of molecular markers, to allow early tumor detection and development of novel and more efficient therapeutic schemes.

In this context, a complex strategy combining high-performance TLC, laser densitometry, and fully automated negative ion mode nanoESI chip coupled to QTOF MS was designed and applied for mapping of gangliosides in a specimen of human angioblastic meningioma [62]. Qualitative analysis of ganglioside pattern using TLC identified GM3, GM2, GM1, GD3, GD1a (nLD1, LD1), GD1b, and GD2 species in human meningioma. Moreover, comparative TLC analyses indicated considerable differences between the proportions of ganglioside species in meningioma vs. healthy brain tissue and showed for the first time that meningioma tissue is rich in GD1a (nLD1, LD1). However, by high resolution MS with chip-based ESI, 34 distinct species, of which two asialo, were identified. This inventory determined by MS contained many more species than previously reported in meningiomas using other biochemical or biophysical methods. Besides the unexpected number of species, an interesting characteristic revealed by MS is the exclusive expression of species with shorter glycan chains and reduced sialic acid content, i.e., maximum sialylation degree found in meningioma is 2.

Another characteristic of meningioma is the absence of *O*-fucosylation, *O*-acetylation, or *O*-GalNAc modification of the main oligosaccharides chain of ganglioside species found in other brain tumors or brains affected by neurodegenerative disorders. Furthermore, nanoESI chip MS evidenced that despite the low percentage of GM1 fraction in meningioma, a number of eight abundant ions were attributable to nine GM1 forms. CID MS/MS analysis documented that both GM1a and GM1b isomers are expressed in meningioma tissue. The findings related to GM1 advocate for the first time that, beside GM3 species, already known as an indisputable marker of meningioma, GM1 class is also associated to this type of tumor.

Hemangioma

Hemangioma represents a congenital benign tumor or vascular malformation of endothelial cells. The ailment features enlarged blood vessels with a single layer of endothelium accompanied by the absence of neuronal tissue within the lesions. Cavernous hemangioma is the most widespread form of brain hemangioma. This type can originate from any part of the brain and can also occur at any location along the vascular bed [28]. Frontal and temporal lobes are the most common sites of occurrence, with approximately 70 % of these lesions located in the supratentorial region of the brain; the remaining 30 % arise in the infratentorial region.

Hemangioma is most usually diagnosed by imaging techniques such as magnetic resonance imaging. A more specific detection can be accomplished by gradient-echo sequence MRI, able to expose even the tiny lacerations [39]. A practical choice to these methods is the early detection of hemangioma at an incipient stage, based on routine screening and cancer biomarker discovery before clinical symptoms arise. As bioindicators of brain cancer, gangliosides in hemangioma were analyzed by mass spectrometry in an attempt to discover the species associated to this type of tumors [61]. Native ganglioside mixture extracted from brain

hemangioma in the frontal cortex of an adult patient was screened by nanoESI chip high capacity ion trap MS in comparison with age-matched healthy frontal cortex. In contrast to the normal tissue, ganglioside mixture extracted from hemangioma was found dominated by species of short oligosaccharide chains with a reduced overall sialic acid content. From a total of 29 structures identified in hemangioma tissue, 13 were monosialylated species of GM1, GM2, GM3, and GM4-type and 13 disialylated species of GD1 and GD2-type bearing ceramides of variable structure. Only two polysialylated species namely GT1 having (d18:1/20:0) ceramide composition and GT3 with (d18:1/25:1) ceramide were detected. However, none of these trisialylated ganglioside forms were detected in the normal tissue; this aspect shows that such components are either absent or much lower expressed in normal frontal lobe, being associated to hemangioma tumor. Interestingly, two modified ganglioside structure were observed in the ganglioside mixture extracted from hemangioma: *O*-Ac-GD2 (d18:1/23:0) and *O*-Ac-GM4 (d18:0/29:0). The same *O*-Ac-GD2 (d18:1/23:0) species was identified also in the normal tissue of the frontal cortex, and was never reported in malignant tumors [61]. This suggested that *O*-Ac-GD2 structures might be markers of either benign cerebral tumors or tumors with reduced malignancy grade.

According to the presented data on meningioma, apparently the expression of polysialylated gangliosides is regulated in a growth- and development-dependent mode and associated with the type of normal/aberrant brain tissue status.

8.4.2.2 Malignant Tumors

Astrocytoma

Astrocytomas (AcTs) are collection of CNS neoplasms characterized by predominant cell type derived from an immortalized astrocyte. Situated in most parts of the brain, sporadically even in the spinal cord, astrocytomas can induce compression, invasion, and destruction of the neural tissue.

AcTs are categorized in four subtypes according to the growth rate and prospective for proliferation in the adjacent brain tissue [42]: (1) pilocytic astrocytoma (grade I), a slow-growing astrocytoma that usually does not spread to other parts of the CNS; (2) low grade astrocytoma (grade II), a relatively slow-growing type, which can invade the surrounding brain tissue and tends to reappear after treatment; (3) anaplastic astrocytoma (grade III) characterized by a rapidly growing rate, with incursion in the normal brain tissue and rapid recurrence after the treatment; (4) glioblastoma multiforme (grade IV), the most aggressive and highly invasive type displaying necrosis areas and a variety of cells including astrocytes and oligodendrocytes.

Astrocytomas have poor survival rates, considered from diagnosis and the beginning of the treatment as follows: 10 years for pilocytic form, 5 years for patients with low-grade diffuse astrocytomas, 2–5 years for anaplastic astrocytomas, and less than 1 year for patients with glioblastoma [87]. Regrettably, astrocytomas affect young ages, the most cases of pilocytic astrocytoma being discovered in the first two decades

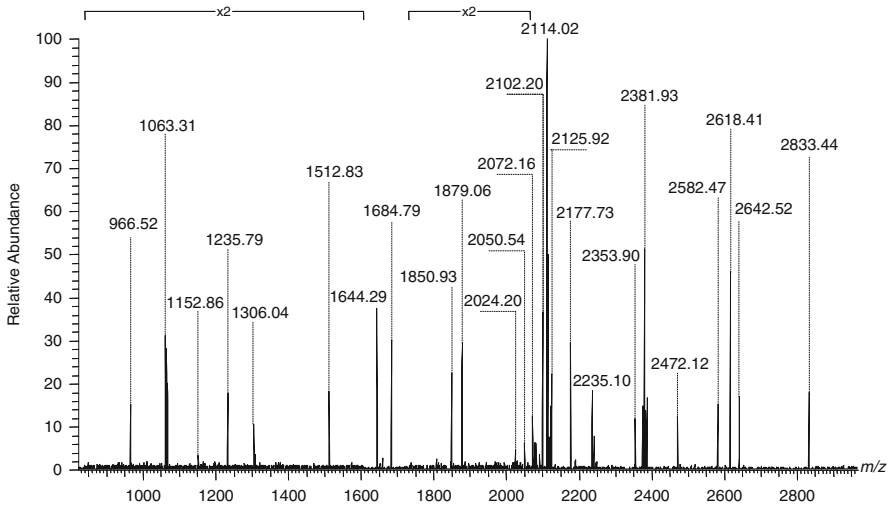

Fig. 8.10 NanoESI Orbitrap MS screening in the negative ion mode of the gangliosides from human astrocytoma. Solvent MeOH. Sample concentration: approximately 2 pmol/μL. Acquisition time 1 min. Flow rate 150 nL/min. Sample volume consumption 150 nL. Spray voltage 1.1 kV. Counterelectrode voltage −35 V. Reprinted with permission from Zamfir et al. [90]

of life [57]. In contrast, low-grade astrocytomas affect especially people aged 30–40 years and, only in low percentage, patients younger than 20 years of age.

Astrocytomas are usually detected by expensive diagnostic imaging methods often in a late phase, when only palliative treatment is possible. The only practical alternative is the early detection of tumor, at a stage when the resection is possible, which should be based on routine screening and biomarker discovery before clinical symptoms arise. Therefore, nowadays, the research is focused on the development of efficient analytical methods able to discover molecular fingerprints, among which the class of gangliosides is the most promising. Based on these premises, in 2013 the first investigation of gangliosides expressed in a low-grade astrocytoma by high-resolution MS on an Orbitrap instrument was initiated [90]. The research was conducted towards the first mapping of gangliosides in specimens from AcT, its surrounding tissue (ST), and a normal control brain tissue from the frontal lobe (NT) under identical conditions. Comparative (−) nanoESI MS screening at a sample concentration of only 2 pmol/μL of gangliosides from AcT (Fig. 8.10), ST (Fig. 8.11), and NT (Fig. 8.12) has led to the following findings summarized in Table 8.5a–c: (1) ganglioside compositions in AcT and ST are altered in comparison to the ganglioside expression in NT; (2) a number of 30 species are associated to the tumor; (3) 14 ganglioside species in AcT, 14 in ST, and only 5 in NT exhibit ceramide moieties with long chain fatty acids exceeding 25 carbon atoms. This finding represents another characteristic distinguishing AcT and ST from NT; (4) ST extract presents high levels of sialylation, fucosylation, and acetylation, typical for malignant transformation, a feature indicating the phenomenon of AcT cells protrusion in the ST.

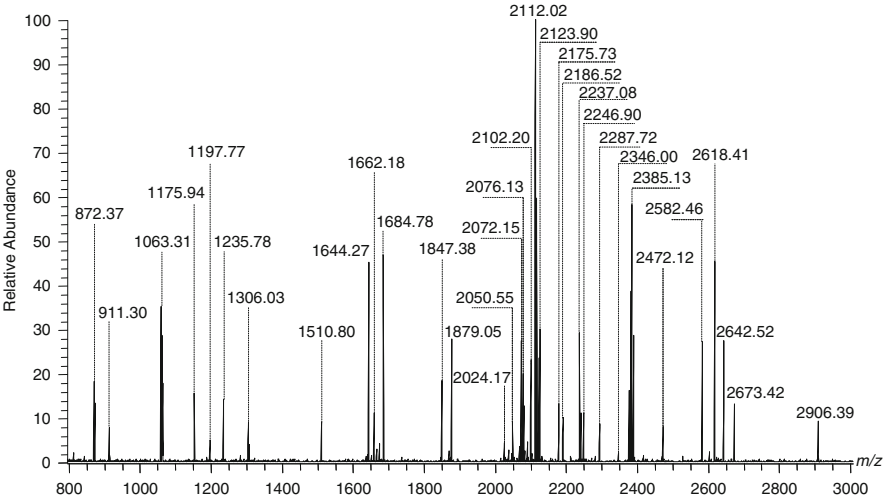

Fig. 8.11 NanoESI Orbitrap MS screening in the negative ion mode of the gangliosides from human astrocytoma surrounding tissue. Conditions as in Fig. 8.10. Reprinted with permission from Zamfir et al. [90]

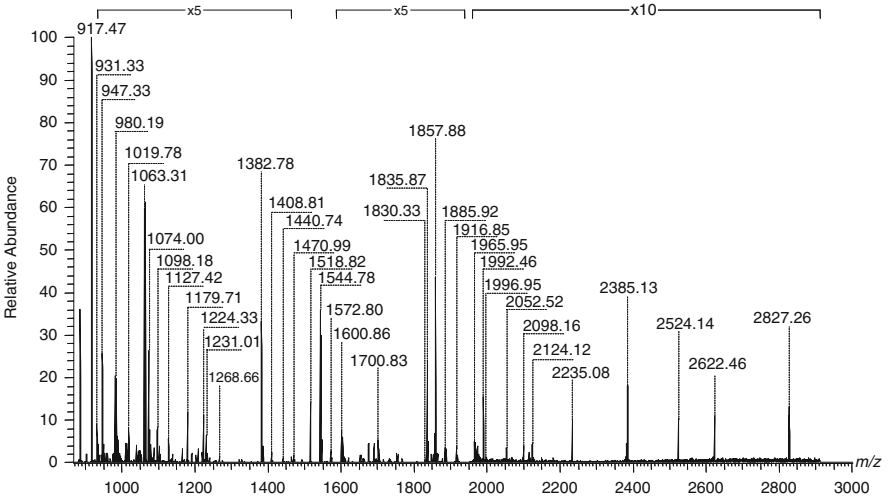

Fig. 8.12 NanoESI Orbitrap MS screening in the negative ion mode of the gangliosides from control tissue originating from the frontal lobe. Conditions as in Fig. 8.10. Reprinted with permission from Zamfir et al. [90]

The MS screening data indicated that AcT, ST, and NT present a common ganglioside structure: GT1(d18:1/18:0) or GT1(d18:0/18:1). CID MS^2–MS^4 experiments (Fig. 8.13) yielded a number of product ions corroborating for the presence of a GT1c isomer (Fig. 8.14) in AcT and ST, but not in NT. A GT1c isomer having

Table 8.5 Proposed composition of single components in the ganglioside mixture from (a) AcT. (b) ST. (c) NT as detected by negative ion mode nanoESI Orbitrap MS

m/z (monoisotopic) experimental	*m/z* (monoisotopic) theoretical	Mass accuracy (ppm)	Molecular ion	Proposed composition
966.52	966.53	10.35	$[M-2H]^{2-}$	GD1, nLD1 and/or LD1 (d18:1/25:0) or (d20:1/23:0)
1,063.31	1,063.33	18.81	$[M-2H]^{2-}$	GT1(d18:1/18:0) or GT1(d18:0/18:1)
1,152.86	1,152.88	17.34	$[M-H]^{-}$	GM3(d18:1/16:0) or GM3(d18:0/16:1)
1,235.79	1,235.81	16.18	$[M-H]^{-}$	GM3 (d18:1/22:0)
1,306.04	1,306.06	15.31	$[M-H]^{-}$	GM3(d18:1/27:0)
1,512.83	1,512.86	19.82	$[M-H]^{-}$	*O*-Ac-GD3 (d18:1/18:0)
1,644.29	1,644.31	12.16	$[M-H]^{-}$	GM1 (d18:0/25:0)
1,684.79	1,684.82	17.80	$[M-H]^{-}$	GD2(d18:1/19:2) or GD2(d18:0/19:3)
1,850.93	1,850.97	21.60	$[M-H]^{-}$	GD1(d18:1/19:0) or GD1(d18:0/19:1)
1,879.06	1,879.10	21.28	$[M-H]^{-}(-H_2O)$	Fuc-GT3(d18:0/17:0) or *O*-Ac-GT3 (d18:2/22:1)
	1,879.09	15.96	$[M+Na-2H]^{-}$	
2,024.20	2,024.24	19.76	$[M+2Na-3H]^{-}$	GD1 (d18:0/28:0)
2,050.54	2,050.60	29.26	$[M-H]^{-}$	GT2(d18:1/24:0) or GT2(d18:0/24:1)
2,072.16	2,072.21	24.13	$[M-H]^{-}$	*O*-Ac-GD1(d18:1/32:1)
2,102.20	2,102.26	28.54	$[M-H]^{-}$	*O*-Ac-GD1(d18:1/34:0)
2,114.02	2,114.09	33.11	$[M-H]^{-}$	GT1(d18:1/17:1) or GT1(d18:0/17:2)
2,125.92	2,125.97	23.51	$[M-H]^{-}$	GT1(d18:1/18:1)
2,177.73	2,177.80	32.13	$[M-H]^{-}$	GT2 (d18:0/33:0)
2,235.10	2,235.16	26.84	$[M-H]^{-}$	GT1(d18:1/26:2)
2,353.90	2,353.97	29.73	$[M+Na-2H]^{-}$	GQ1 (d18:1/12:1)
2,381.93	2,382.01	33.58	$[M+Na-2H]^{-}$	GQ1 (d18:1/14:1)
2,472.12	2,472.21	36.40	$[M-H]^{-}$	GQ1(d18:1/22:1)
2,582.47	2,582.56	34.84	$[M-H]^{-}(-H_2O)$	GQ1(d18:1/31:0)
2,618.41	2,618.51	38.18	$[M+2Na-3H]^{-}$	GQ1(d18:0/29:0)

(continued)

Table 8.5 (continued)

m/z (monoisotopic) experimental	*m/z* (monoisotopic) theoretical	Mass accuracy (ppm)	Molecular ion	Proposed composition
2,642.52	2,642.62	37.83	$[M-H]^-$	*O*-Ac-GQ1(d18:1/31:0)
2,833.44	2,833.55	38.82	$[M-H]^-$	GP1(d18:1/27:1)
872.37	872.38	11.46	$[M-2H]^{2-}$	*O*-Ac-GD2 (d18:1/20:0)
911.30	911.31	10.97	$[M-2H]^{2-}$	GD1, nLD1 or LD1 (d18:1/18:3)
1,063.31	1,063.33	18.81	$[M-2H]^{2-}$	GT1(d18:1/18:0) or GT1(d18:0/18:1)
1,175.94	1,175.96	17.00	$[M-H]^-$	GM3 (d18:1/18:2)
1,197.77	1,197.80	25.04	$[M-H]^-$	GM3(d18:0/19:0)
1,235.78	1,235.81	24.29	$[M-H]^-$	GM3 (d18:1/22:0)
1,306.03	1,306.06	22.97	$[M-H]^-$	GM3(d18:1/27:0)
1,510.80	1,510.84	26.47	$[M-H]^-$	*O*-Ac-GD3 (d18:1/18:1)
1,644.27	1,644.31	24.33	$[M-H]^-$	GM1 (d18:0/25:0)
1,662.18	1,662.22	24.06	$[M-H]^-$	GM1 (d18:1/29:2)
1,684.78	1,684.82	23.73	$[M-H]^-$	GD2(d18:1/19:2) or GD2(d18:0/19:3)
1,847.38	1,847.42	21.65	$[M-H]^-$	GT3(d18:0/24:0)
1,879.05	1,879.09	21.28	$[M-H]^-(-H_2O)$	Fuc-GT3(d18:0/17:0) or *O*-Ac-GT3 (d18:1/22:2)
	1,879.10	26.60	$[M+Na-2H]^-$	
2,024.17	2,024.23	29.64	$[M+2Na-3H]^-$	GD1 (d18:0/28:0)
2,050.55	2,050.60	24.37	$[M-H]^-$	GT2(d18:1/24:0) or GT2(d18:0/24:1)
2,072.15	2,072.21	28.95	$[M-H]^-$	*O*-Ac-GD1(d18:1/32:1)
2,076.13	2,076.19	28.90	$[M-H]^-$	*O*-Ac-GD1(d18:0/32:0)
2,102.20	2,102.26	28.54	$[M-H]^-$	*O*-Ac-GD1(d18:1/34:0)
2,112.02	2,112.09	33.14	$[M-H]^-$	GT1(d18:1/17:2) or GT1(d18:0/17:3)
2,123.90	2,123.97	32.95	$[M-H]^-$	GT1(d18:1/18:2)
2,175.73	2,175.80	32.16	$[M-H]^-$	GT2 (d18:1/33:0)
2,186.52	2,186.60	36.57	$[M-H]^-$	GT1(d18:0/22:0)
2,237.08	2,237.16	35.76	$[M-H]^-$	GT1(d18:1/26:1)

2,246.90	2,246.98	35.60	$[M-H]^-$	Fuc-GT1(d18:0/16:0)
2,287.72	2,287.80	34.96	$[M-H]^-$	Fuc-GT1 (d18:0/20:0)
2,346.00	2,346.09	38.36	$[M-H]^-$ $(-H_2O)$	GQ1(d18:1/13:1)
2,385.13	2,385.22	37.73	$[M+3Na-4H]^-$	GT1(18:1/32:2)
2,472.12	2,472.21	36.40	$[M-H]^-$	GQ1(d18:1/22:1)
2,582.46	2,582.56	38.71	$[M-H]^-$ $(-H_2O)$	GQ1(d18:1/31:0)
2,618.41	2,618.51	38.18	$[M+2Na-3H]^-$	GQ1(d18:0/29:0)
2,642.52	2,642.62	37.83	$[M-H]^-$	*O*-Ac-GQ1(d18:1/31:0)
2,673.42	2,673.52	37.41	$[M-H]^-$	GP2(d18:1/27:0)
2,906.39	2,906.50	37.85	$[M-H]^-$	Fuc-GP1(d18:1/23:1)
917.47	917.48	10.90	$[M-2H]^{2-}$	GD1, nLD1 or LD1 (d18:1/18:0)
931.33	931.34	10.74	$[M-2H]^{2-}$	GD1, nLD1 or LD1 (d18:1/20:0)
947.33	947.34	10.55	$[M-H]^-$	LacCer (d18:0/22:0)
980.19	980.21	20.40	$[M+Na-2H]^-$	GM4 (d18:1/14:2)
1,019.78	1,019.80	19.60	$[M-2H]^{2-}$	GT2 (d18:1/22:2)
1,063.31	1,063.33	18.81	$[M-2H]^{2-}$	GT1(d18:1/18:0) or GT1(d18:0/18:1)
1,074.00	1,074.02	18.62	$[M+Na-3H]^{2-}$	GT1 (d18:1/18:0)
1,098.18	1,098.20	18.21	$[M-2H]^{2-}$	GT1(d18:1/23:0) or GT1(d18:0/23:1)
1,127.42	1,127.45	26.61	$[M+Na-2H]^-$	GM3 (d18:1/13:2)
1,179.71	1,179.74	25.42	$[M-H]^-$	GM3(d18:1/18:0)
1,224.33	1,224.36	24.50	$[M-H]^-$	Fuc-GM3 (d18:1/12:0)
1,231.01	1,231.04	24.37	$[M+2Na-4H]^{2-}$	GQ1 (d18:1/18:0)
1,268.66	1,268.69	23.64	$[M-H]^-$	GM2 (d18:1/10:0)
1,382.78	1,382.82	28.92	$[M-H]^-$	GM2 (d18:1/18:0)
1,408.81	1,408.85	28.38	$[M-H]^-$	GM2 (d18:1/20:1)
1,440.74	1,440.78	27.75	$[M-H]^-$	GD3 (d18:1/16:1)
1,470.99	1,471.03	27.19	$[M-H]^-$	GD3 (d18:1/18:0)
1,518.82	1,518.86	26.33	$[M-H]^-$	GM1(d18:0/16:0)

(continued)

Table 8.5 (continued)

m/z (monoisotopic) experimental	*m/z* (monoisotopic) theoretical	Mass accuracy (ppm)	Molecular ion	Proposed composition
1,544.78	1,544.83	32.36	$[M-H]^-$	GM1, nLM1 or LM1 (d18:1/18:0)
1,572.80	1,572.85	31.78	$[M-H]^-$	GM1, nLM1 or LM1 (d18:1/20:0)
1,600.86	1,600.92	37.47	$[M-H]^-$	GM1,nLM1or LM1 (d18:1/22:0)
1,700.83	1,700.89	35.27	$[M+2Na-3H]^-$	GM1(d18:1/26:0)
1,830.33	1,830.40	38.25	$[M-H]^-$	GT3 (d18:1/23:1)
1,835.87	1,835.94	38.12	$[M-H]^-$	GD1, nLD1or LD1(d18:1/18:0)
1,857.88	1,857.95	37.67	$[M+Na-2H]^-$	GD1, nLD1 or LD1 (d18:1/18:0)
1,885.92	1,885.99	37.11	$[M+Na-2H]^-$	GD1(d18:1/20:0)
1,916.85	1,916.92	36.51	$[M-H]^-$	GD1 (d18:1/24:2)
1,965.95	1,966.02	35.60	$[M-H]^-$	GT2(d18:1/18:1) or GT2(d18:0/18:2)
1,992.46	1,992.53	35.12	$[M-H]^-$	Hex-HexNAc-nLM1(d18:1/24:1)
1,996.95	1,996.96	35.05	$[M-H]^-$	GD2–lactone (d18:1/22:2)
2,052.52	2,052.60	38.96	$[M-H]^-$	GT2 (d18:0/24:0)
2,098.16	2,098.24	38.13	$[M-H]^-$	*O*-Ac-GD1(d18:1/34:2)
2,124.12	2,124.20	37.66	$[M-H]^-$	GT1(d18:1/18:2) or GT1(d18:0/18:3)
2,235.08	2,235.16	35.79	$[M-H]^-$	GT1(d18:1/26:2)
2,385.13	2,385.22	37.73	$[M+3Na-4H]^-$	GT1(18:1/32:2)
2,524.14	2,524.24	39.61	$[M+Na-2H]^-$	GQ1(d18:1/24:0)
2,622.46	2,622.56	38.12	$[M+Na-2H]^-$	GQ1(d18:1/31:0)
2,827.26	2,827.37	38.91	$[M-H]^-(-H_2O)$	GP1(d18:1/28:2)

Reprinted with permission from [90]

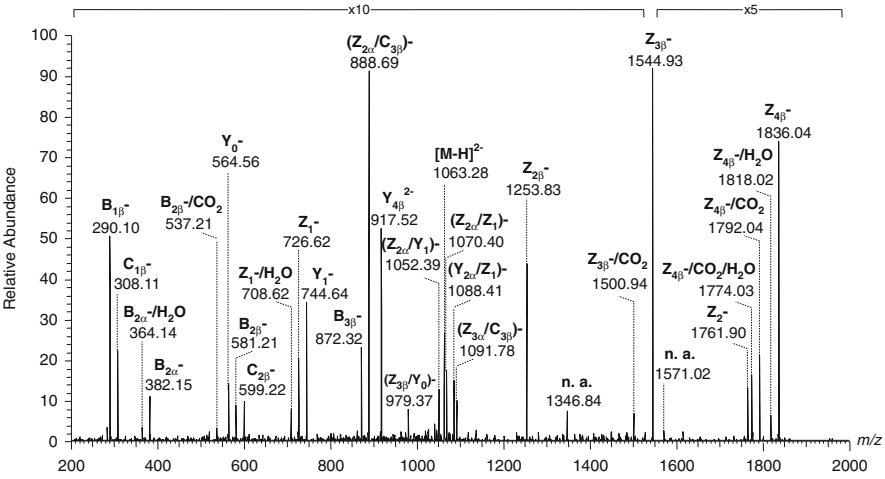

Fig. 8.13 Structural analysis by CID MS^2 of the $[M-2H]^{2-}$ corresponding to GT1(d18:1/18:0) or GT1(d18:0/18:1) detected at *m/z* 1.063.28 by MS screening of astrocytoma gangliosides. Collision energy within 35–50 eV range (*Elab*). The assignment of the fragment ions is according to the nomenclature [14]. Reprinted with permission from Zamfir et al. [90]

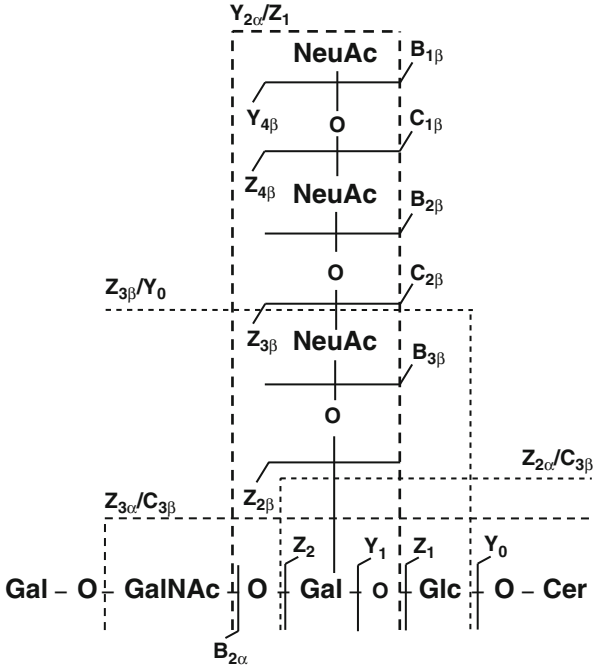

Fig. 8.14 Fragmentation scheme of GT1c (d18:1/18:0) or GT1c (d18:0/18:1) by CID MS^2. The assignment of the fragment ions is according to the nomenclature [14]. Reprinted with permission from Zamfir et al. [90]

(d18:1/18:0) ceramide composition was never identified in another brain tumor, which shows that under the high-resolution conditions and multiple stage fragmentation on Orbitrap MS, a novel species, biomarker of human astrocytoma was discovered and structurally characterized.

Gliosarcoma

Glioblastoma multiforme is a rare primary neoplasm of the CNS, ranked by the World Health Organization as a grade IV tumor [42]. Gliosarcoma is a variant of glioblastoma multiforme [25] defined by a biphasic tissue pattern consists of alternating areas displaying glial and mesenchymal (sarcomatous) differentiation. Gliosarcoma accounts for about 2 % of all the glioblastomas, usually affecting the adult population in the fourth to the sixth decade of life with a prevalence in male population (male:female, 1.8:1).

Gliosarcomas are usually located in the cerebral cortex involving the temporal, frontal, parietal, and occipital lobe in decreasing frequency. The typical clinical history of the patient is short and the presenting symptoms depend upon the location of the tumor [25]. Even after radical resection by surgery followed by chemo- and radiotherapy, the median survival time is usually 11.5 months with less than 10 % survival after 2 years following diagnosis [44]. The failure of the present therapeutic scheme in glioblastoma is the tumor aggressiveness which leads to rapid infiltration of the tumoral cells into the adjacent healthy brain tissue, which makes them rather inaccessible to treatment methods. Therefore, the present strategies investigated for treatment is to target the invading tumor cells by using specific binding ligands [68]. The critical point is, however, to identify the tumor-specific target molecules and characterize their structures in detail.

In the case of human gliomas, mono- and di-sialylated ganglioside species have been suggested as associated species and/or antigens [19]. Although by various methods a few gangliosides were found potential candidates as glioma-antigens, a more comprehensive mapping of this tumor biomarkers could be achieved by high-resolution mass spectrometry using chip-based nanoESI QTOF and ESI FTICR MS for screening and CID for structural elucidation [83]. By these accurate methods it was found that ganglioside expression in gliosarcoma is highly altered as compared to the normal brain. For instance, GD3 species having d18:1/18:0, d18:1/24:1, and d18:1/24:0 Cer compositions were found dominant in the ganglioside mixture extracted from human gliosarcoma (Fig. 8.15). Unexpectedly a high abundance of *O*-acetylated GD3 derivatives, particularly with d18:1/18:0 and d18:1/20:0 lipid moiety structure, were also observed. GM2, GM1, and/or their isomers nLM1 and LM1, as well as GD1 species characterized by heterogeneity in composition of their ceramide moieties, were found abundantly in the mixture, while the species with a higher sialylation degree were found poorly or not at all expressed. The reduction in the total ganglioside content and the altered pattern in gliosarcoma vs. control tissue is considered the result of both a lower overall biosynthetic rate, due to change in expression of certain glycosyltransferases, and higher turnover rate [83].

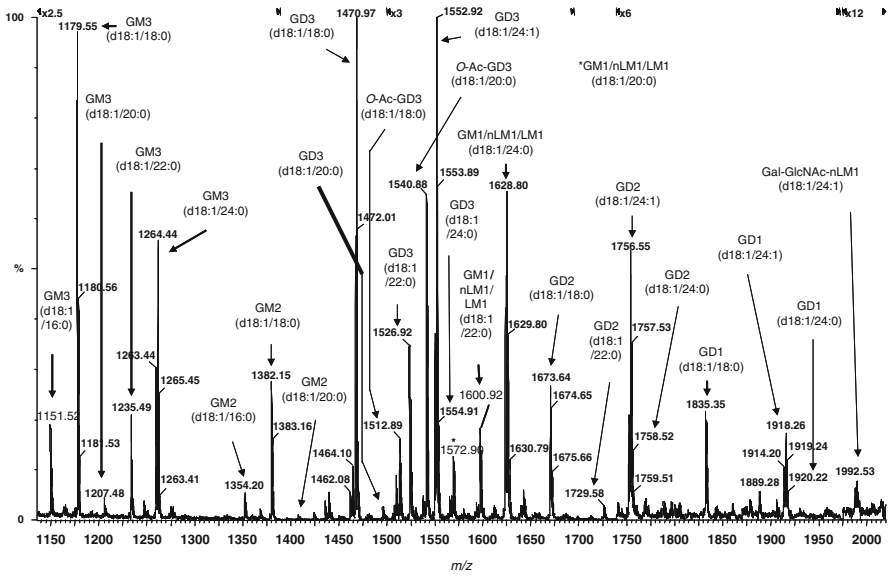

Fig. 8.15 NanoESI chip QTOF MS of the native gliosarcoma ganglioside mixture. ESI voltage 1.60 kV. Sampling cone 80 V. Acquisition 2 min. Average sample consumption 0.5 pmol. Reprinted with permission from Vukelić et al. [83]

A higher expression of sialyltransferase II (GD3 synthase) and a lower expression of galactosyltransferase II were found to be the most probable causes of the very high GD3 and very low GM1a, GD1a, and GD1b abundances. While the latter species were previously known as glioma biomarkers, GD3 and the corresponding acetylated forms were discovered only by mass spectrometry as tumor-associated. Tandem MS by CID using as the precursor *O*-Ac-GD3 (Fig. 8.16) provided sequence data consistent with the presence of gliosarcoma-associated isomer bearing *O*-acetylation at the inner Neu5Ac residue, a form previously not structurally confirmed. The information derived from the MS data according to which gliosarcoma, as the highest malignancy grade brain tumor, contains a higher amount of potentially proapoptotic GD3 than of the *O*-acetyl GD3 species suports the previous assumption [33] that the role of *O*-Ac-GD3 as tumor-specific component is the protection of tumor cells from apoptosis.

8.4.3 Secondary Brain Tumors

When highly expressed, some of the glycosyl epitopes promote invasion and metastasis and thus can lead to shorter survival rate of patients, while some others suppress tumor progression leading to higher postoperative survival period. Targeting carbohydrate antigens such as gangliosides expressed on metastatic tumor cells

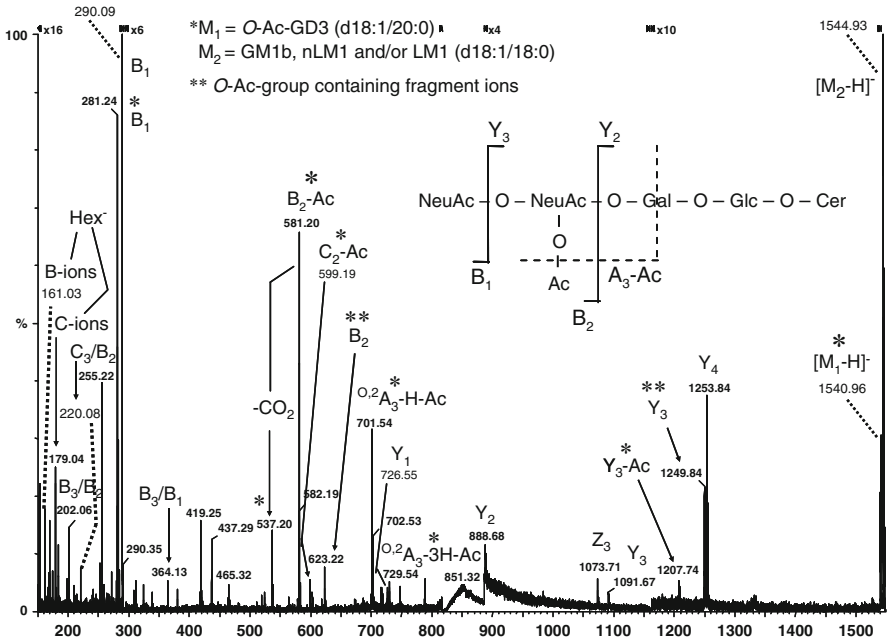

Fig. 8.16 NanoESI QTOF CID MS/MS of the $[M-H]^-$ at *m/z* 1,540.96 corresponding to the *O*-Ac-GD3 (d18:1/20:0). ESI voltage 1,000–1,250 V. Collision energy 25–40 eV. Collision gas pressure 5–10 psi. Acquisition time 11 min. Average sample consumption 3.5 pmol. Inset: the fragmentation scheme of *O*-Ac-GD3. Reprinted with permission from Vukelić et al. [83]

represents a priority for the immunotherapy of cancer since aberrant glycosylation exhibited by tumor cells is considered a factor of their uncontrolled growth, invasiveness, and increased metastatic potential.

8.4.3.1 Brain Metastasis of Lung Adenocarcinoma

Lung adenocarcinoma is a histological form of lung cancer that contains certain distinct malignant tissue architectural, cytological, or molecular features. Non-small cell lung cancer, the most frequent cause of cancer deaths in many countries, has a high risk of brain metastases that reportedly reaches 44 % in brain autopsy. As compared to other primary cancers, where brain spread is usually a later complication, lung cancer develops intracranial metastases relatively early and is often accompanied by neurologic symptoms on initial diagnosis [22].

Untreated brain metastases have a median survival of about 4 weeks with almost all patients dying from neurological rather than systemic causes [2]. Whole-brain radiation therapy and chemotherapy are currently the standard, unfortunately only palliative, treatments for patients with brain metastases. Even under treatment, the prognosis for patients with brain metastases is generally poor, with median survival time between 3 and 6 months [20].

Table 8.6 Ganglioside and asialo-ganglioside species from brain metastasis of lung adenocarcinoma (male, 73 years) detected by negative ion mode nanoESI chip QTOF MS analysis of complex native ganglioside mixture

m/z (monoisotopic) theoretical	*m/z* (monoisotopic) experimental	Mass accuracy (ppm)	Molecular ion	Proposed structure
875.19	874.91	33	$[M-H]^-$	LacCer(d18:1/17:0)
933.31	932.99	35	$[M-H]^-$	LacCer(d18:0/21:0)
947.34	947.19	16	$[M-H]^-$	LacCer(d18:0/22:0)
949.22	949.24	21	$[M+2Na-3H]^-$	LacCer(d18:0/19:0)
964.24	963.90	35	$[M-H]^-$	GM4(d18:0/14:0)
982.19	981.94	25	$[M+Na-2H]^-$	GM4(d18:1/14:1)
984.21	983.87	34	$[M+Na-2H]^-$	GM4(d18:1/14:0) or GM4(d18:0/14:1)
1,122.48	1,122.23	22	$[M-H]^-$	GA2(d18:0/20:0)
1,138.44	1,138.15	25	$[M-H]^-$	Fuc-GM4(d18:0/16:0) GA2(t18:0/20:0)
1,138.48		29		
1,150.49	1,150.17	28	$[M-H]^-$	GA2(d18:1/21:0)
1,150.40		20	$[M-H]^-$	GM3(d18:1/16:1)
1,168.42	1,168.01	35	$[M-H]^-$	GM3(t18:0/16:0)
1,178.46	1,178.14	27	$[M-H]^-$	GM3(d18:1/18:1)
1,179.74	1,180.10	30	$[M-H]^-$	GM3(d18:1/18:0)
1,182.49	1,182.21	24	$[M-H]^-$	GM3(d18:0/18:0)
1,184.37	1,184.08	24	$[M-H]^-$	*O*-Ac-GA1(d18:1/10:0)
1,194.50	1,194.15	29	$[M-H]^-$	GM3(d18:1/19:0) or GM3(d18:0/19:1)
1,206.51	1,206.33	15	$[M-H]^-$	GM3(d18:1/20:1)
1,206.64		26	$[M-H]^-$	GA2(d18:0/26:0)
1,222.51	1,222.19	26	$[M-H]^-$	*O*-Ac-GM3(d18:1/18:0)
1,222.55		29	$[M-H]^-$	GM3(d18:0/21:1) or GM3(d18:1/21:0)
1,234.56	1,234.22	27	$[M-H]^-$	GM3(d18:1/22:1)
1,234.52		24		*O*-Ac-GM3(d18:1/19:1)

(continued)

Table 8.6 (continued)

m/z (monoisotopic) theoretical	*m/z* (monoisotopic) experimental	Mass accuracy (ppm)	Molecular ion	Proposed structure
1,248.55	1,248.18	33	$[M-H]^-$	*O*-Ac-GM3(d18:1/20:1)
1,248.59		30		GM3(d18:1/23:1)
1,248.59	1,249.02	34	$[M-H]^-$	GM3(d18:1/23:0)
1,260.60	1,260.33	21	$[M-H]^-$	GM3(d18:1/24:2)
1,262.62	1,262.35	21	$[M-H]^-$	GM3(d18:1/24:1)
1,264.63	1,264.19	35	$[M-H]^-$	GM3(d18:1/24:0)
1,276.61	1,277.01	31	$[M-H]^-$	*O*-Ac-GM3(d18:1/22:0)
1,276.64		29	$[M-H]^-(-H_2O)$	GM3(d20:1/23:1)
1,276.69		25		GM3(d18:0/26:0)
1,278.66	1,278.21	35	$[M-H]^-$	GM3(d20:1/23:0)
1,278.61		31	$[M-H]^-$	*O*-Ac-GM3(d18:1/22:0) or *O-Ac-GM3*(d18:0/22:1)
1,288.67	1,289.04	29	$[M-H]^-$	GM3(d18:1/26:2) or GM3(d18:2/26:1)
1,288.67		29	$[M-H]^-$	GM3(d20:1/24:2)
1,292.68	1,292.23	35	$[M-H]^-$	GM3(d18:1/26:0) or GM3(d18:0/26:1)
1,296.54	1,296.24	23	$[M-H]^-$	Fuc-GM3(d18:1/16:1)
1,296.59		27	$[M-H]^-$	*O*-Ac-GA1(d18:1/18:0)
1,296.61		28	$[M-H]^-$	GA1(d18:0/21:0) or GA1(d18:0/21:0)
1,405.65	1,405.21	31	$[M+Na-2H]^-$	GM2(d18:1/18:0)
1,420.68	1,420.80	8	$[M-H]^-$	*O*-Ac-GM2(d18:2/18:2)
1,435.59	1,435.21	26	$[M+Na-2H]^-$	GD3(d18:1/14:1) or GD3(d18:0/14:2) or GD3(d18:2/14:0)
1,441.66	1,441.19	33	$[M-H]^-$	GD3(d18:1/16:1) or GD3(d18:0/16:2) or GD3(d18:2/16:0)
1,471.73	1,471.28	31	$[M-H]^-$	GD3(d18:1/18:0)
1,493.71	1,493.23	32	$[M+Na-2H]^-$	GD3(d18:1/18:0)
1,515.69	1,515.29	26	$[M+2Na-3H]^-$	GD3(d18:1/18:0) or GD3(d18:0/18:1)
1,515.74		30	$[M-H]^-$	GM1(d18:1/16:1) or GM1(d18:0/16:2) or GM1(d18:2/16:0)
1,515.78		32	$[M-H]^-$	*O*-Ac-GD3(d18:0/18:0)

1,515.71	1,516.01	20	$[M+Na-2H]^-$	GD3(d18:1/20:2) or GD3(d18:0/20:3) or GD3(d18:2/20:1)
1,515.75		17	$[M-H]^-$	GM1(d18:2/16:0) or GM1(d18:1/16:1) GM1(d18:0/16:2
1,527.83	1,528.16	22	$[M-H]^-$	GD3(d18:0/22:0)
1,541.79	1,542.19	26	$[M-H]^-$	GM1(d18:1/18:2) or GM1(d18:2/18:1) or GM1(d18:0/18:3)
1,569.78	1,570.29	32	$[M+2Na-3H]^-$	GD3(d18:1/22:0) or GD3(d18:0/22:1)
1,569.83		29	$[M-H]^-$	GM1(d18:1/20:1) or GM1(d18:0/20:2) or GM1(d18:2/20:0)
1,569.77		33	$[M+Na-2H]^-$	GD3(d18:0/24:2) or GD3(d18:1/24:1) or GD3(d18:2/24:0)
1,597.88	1,598.09	13	$[M-H]^-$	GM1(d18:0/22:2) or GM1(d18:1/22:1) or GM1(d18:2/22:0)
1,611.77	1,612.17	25	$[M+2Na-3H]^-$	GM1(d18:1/20:2)
1,625.89	1,625.40	30	$[M+2Na-3H]^-$	GD3(d18:1/26:1) or GD3(d18:0/26:2) or GD3(d18:2/26:0)
1,624.92		30	$[M-H]^-$	GM1(d18:1/24:2)
1,627.90	1,627.41	30	$[M+2Na-3H]^-$	GD3(d18:0/26:1) or GD3(d18:1/26:0)
1,626.93		29	$[M-H]^-$	GM1(d18:0/24:2) or GM1(d18:1/24:1) or GM1(d18:2/24:0)
1,629.92	1,629.42	31	$[M-H]^-$	GM1(d18:0/24:1) or GM1(d18:1/24:0)
1,628.94		29	$[M-H]^-$	di-*O*-Ac-GM1(d18:1/18:0)
1,659.79	1,660.18	23	$[M+3Na-4H]^-$	GM1(d18:1/22:3) or GM1(d18:0/22:4) or GM1(d18:2/22:2)
1,674.87	1,675.23	21	$[M+Na-2H]^-$ $(-H_2O)$	GD2 (d18:1/18:2)
1,748.97	1,749.39	24	$[M+Na-2H]^-$	GD2 (d18:1/22:1)
1,766.97	1,767.28	18	$[M-H]^-$ $(-H_2O)$	GT3 (d18:1/20:1)
1,785.07	1,785.37	17	$[M-H]^-$	*O*-Ac-GD2(d18:1/23:0) or *O-Ac-GD2*(d18:0/23:1)
1,833.81	1,833.28	29	$[M-H]^-$	GT3(d18:0/23:0)
1,833.07		11	$[M-H]^-$	*O*-Ac-GT3 (d18:0/20:0)
1,861.12	1,861.24	6	$[M-H]^-$	*O*-Ac-GT3-lactone(d18:0/22:0)
1,861.12		6	$[M-H]$ $(-H_2O)$	*O*-Ac-GT3(d18:0/22:0)
1,879.09	1,879.39	16	$[M+Na-2H]^-$	*O*-Ac-GT3 (d18:2/22:1)
1,879.10		15	$[M-H]^-(-H_2O)$	Fuc-GT3(d18:0/17:0)
1,879.99		32	$[M-H]^-$	GT2(d18:1/12:1) or GT2(d18:2/12:0)

(continued)

Table 8.6 (continued)

m/z (monoisotopic) theoretical	*m/z* (monoisotopic) experimental	Mass accuracy (ppm)	Molecular ion	Proposed structure
1,909.16	1,909.03	7	$[M-H]^-$	GD1 (d18:1/22:0)
1,960.21	1,959.84	19	$[M-H]^-$ ($-2H_2O$)	GT2(d18:0/20:0)
1,960.12		14	$[M-H]^-$	GT2(d18:1/18:3) or GT2(d18:2/18:2)
1,990.17	1,989.78	20	$[M+Na-2H]^-$	GT2(d18:0/18:0)
1,990.19		21	$[M-H]^-$	GT2(d18:0/20:3) or GT2(d18:1/20:2) or GT2(d18:2/20:1)
1,990.19	1,990.83	32	$[M-H]^-$	GT2(d18:1/20:1) or GT2(d18:0/20:2) or GT2(d18:2/20:0)
2,005.20	2,005.63	21	$[M-H]^-$	Fuc-GD1(d18:1/20:2)
2,006.19		28		*O*-Ac-GT2(d18:1/18:1)
2,048.23	2,048.80	28	$[M-H]^-$	di-*O*-Ac-GT2(d18:0/18:0)
2,048.10		34	$[M-H]^-(-H_2O)$	GT1(d18:2/14:2) or GT1(d18:3/14:1)

Reprinted with permission from [89]

Non-small cell lung cancer has been shown to exhibit elevated expression of GM3 and GM3 synthase (sialyltransferase-I or SAT-I) mRNA with a positive correlation between expression levels of SAT-I mRNA and GM3 in tumor tissues [51]. Overexpression of GM3 synthase was used to determine the effects of endogenous gangliosides on the metastatic process of 3LL Lewis lung carcinoma cells. It is also known that metastatic potential of lung cancer cells is regulated via GM1 ganglioside by modulating the matrix metalloproteinase-9. Low GM1 expressing cell lines showed increased proliferation, invasion, and metastatic potential [91]. Another ganglioside used in development of novel therapies for small cell lung cancer is fucosyl-GM1, which is specifically expressed in lung cancer cells. In the last year, a bidomainal fucosyl-GM1 ganglioside-based vaccine for the treatment of small cell lung cancer was developed [75]. It was also shown that an anti-ganglioside-based cancer vaccine containing 1E10 anti-idiotypic monoclonal antibody induces apoptosis and antiangiogenic effects in a metastatic lung carcinoma [13].

In 2011 high-performance MS was employed for the investigation of ganglioside expression and structure in secondary brain tumors, i.e., brain metastasis of lung adenocarcinoma [89]. Comparative nanoESI chip QTOF MS screening of gangliosides from metastatic (Table 8.6) vs. healthy tissue (Table 8.7) showed considerable discrepancy in expression, structure, and relative abundances of individual species. In contrast to healthy cerebellar tissue, the ganglioside mixture extracted from brain metastasis of lung adenocarcinoma was found to contain mostly species of short oligosaccharide chains and reduced overall sialic acid content. More than a half, from the total of 63 different ions detected and corresponding to 141 possible structures in brain metastatic tissue, represents monosialylated species of GM1, GM2, GM3, and GM4-type. Besides the large number of monosialylated components, six asialo species of GA1 and GA2-type bearing ceramides of variable constitution were discovered. The observed differences in ceramide structures and alteration of sialylation patterns were attributed to tumor-related changes in human carcinomas.

GD1, GD2, and GD3 as well as GT1, GT2, and GT3 with short carbohydrate chains, expressing different ceramide portions, were also identified in the mixture. Ganglioside components modified by Fuc or *O*-Ac could also be detected, but in a different pattern than in healthy brain; most *O*-acetylated gangliosides were found as monosialo species of GM3, GM2, and GM1 type, while fucosylated components were represented by monosialo species of GM3 and GM4 structure, di- and trisialylated GD1 and GT3 exhibiting high heterogeneity in their ceramide motifs [89].

By tandem MS using CID, brain metastasis-associated GD3 (d18:1/18:0) species was structurally elucidated (Fig. 8.17a, b). This structure was reported to enhance tumor cell proliferation, invasion, and metastasis in a variety of brain tumor cells, especially in glioma and neuroblastoma.

From the methodological point of view it is to be mentioned that nanoESI chip QTOF MS and CID MS/MS was able to provide compositional and structural characterization of native ganglioside mixtures from secondary brain tumors with remarkable analysis speed and sensitivity. Under the applied conditions a sample concentration of only 2.5 pmol/μL, which corresponds to 250 fmol biological extract consumption, was necessary for an experiment.

Table 8.7 Ganglioside and asialo-ganglioside species from the control healthy cerebellum (male, 79 years) detected by negative ion mode nanoESI chip QTOF MS analysis of complex native ganglioside mixture (from [89])

m/z (monoisotopic) theoretical	*m/z* (monoisotopic) experimental	Mass accuracy (ppm)	Molecular ion	Proposed structure
708.35	708.38	4	$[M-3H]^{3-}$	GT1(d18:1/18:0)
714.42	714.40	3	$[M-3H]^{3-}$	GT1(t18:0/18:0)
			$[M+Na-4H]^{3-}$	GT1(d18:1/18:2)
717.58	717.54	5	$[M-3H]^{3-}$	GT1(d18:1/20:0) or GT1(d18:0/20:1)
734.91	735.12	29	$[M-2H]^{2-}$	GD3(d18:1/18:0) or GD3(d18:0/18:1)
756.38	756.30	11	$[M-2H]^{2-}$	*O*-Ac-GD3(d18:1/18:0)
771.95	771.93	3	$[M-2H]^{2-}$	GM1(d18:0/18:1) or GM1(d18:1/18:0)
822.05	822.06	1	$[M+Na-4H]^{3-}$	GQ1(d18:1/20:0) or GQ1(d18:0/20:1)
835.95	835.69	31	$[M-2H]^{2-}$	GD2(d18:1/18:1) or GD2(d18:0/18:2) or GD2(d18:2/18:0)
844.96	844.69	32	$[M-2H]^{2-}$	*O*-Ac-GD2(d18:0/16:0)
850.47	850.22	29	$[M-2H]^{2-}$	GD2 (d18:1/20:0)
863.51	863.21	35	$[M-2H]^{2-}$	Fuc-GM1(d18:1/22:2) or Fuc-GM1(d18:0/22:3) or Fuc-GM1(d18:2/22:1)
863.00		24	$[M-2H]^{2-}$	GD2(d18:0/22:3) or GD2(d18:1/22:2) or GD2(d18:2/22:1)
862.99		26	$[M+Na-3H]^{2-}$	GD2(d18:0/20:0)
878.03	877.88	17	$[M-2H]^{2-}$	GD2(d18:1/24:1)
886.03	885.78	28	$[M-2H]^{2-}$	*O*-Ac-GD2(d18:1/22:0) or *O*-Ac-GD2(d18:0/22:1)
890.97	890.76	24	$[M+Na-3H]^{2-}$	GT3(d18:1/18:1)
905.01	905.11	11	$[M+Na-3H]^{2-}$	GT3(d18:1/20:0)
917.48	917.44	4	$[M-2H]^{2-}$	GD1(d18:1/18:0) or GD1(d18:0/18:1)
924.49	924.76	29	$[M-2H]^{2-}$	GD1(d18:1/19:0) or *O*-Ac-GT3(t18:1/20:0) or
924.53		25	$[M+2Na-4H]^{2-}$	*O*-Ac-GT3(d18:0/20:1)
931.49	931.45	4	$[M-2H]^{2-}$	GD1(d18:1/20:0) or GD1(d18:0/20:1)
940.50	940.46	4	$[M-2H]^{2-}$	GD1(t18:0/20:0)
940.19		29	$[M+2Na-4H]^{2-}$	GD1 (d18:1/18:0) or GD1(d18:0/18:1)
945.51	945.50	1	$[M-2H]^{2-}$	GD1(d18:1/22:0)

952.52	952.50	2	$[M-2H]^{2-}$	*O*-Ac-GD1 (d18:1/20:0) or *O*-Ac-GD1 (d18:0/20:1)
968.03	968.34	32	$[M-3H]^{3-}$	GH2(d18:1/24:0) or GH2(d18:0/24:1)
991.56	991.27	29	$[M+Na-3H]^{2-}$	GT2(d18:1/18:2) or GT2(d18:0/18:3) or GT2(d18:2/18:3)
1,005.58	1,005.28	30	$[M+2Na-4H]^{2-}$	GT2 (d18:0/18:0)
1,019.02	1,019.36	33	$[M-2H]^{2-}$	GalNAc-GD1(d18:0/18:0)
1,024.62	1,024.68	6	$[M-2H]^{2-}$	di-*O*-Ac-GT2 (d18:1/18:0)
1,024.57		11	$[M+2Na-4H]^{2-}$	*O*-Ac-GT2 (d18:1/18:1)
1,034.24	1,033.94	29	$[M+2Na-3H]^{-}$	GM4 (d18:1/16:0) or GM4 (d18:0/16:1)
1,042.60	1,042.51	9	$[M-2H]^{2}$	GT1 (t18:1/14:1) or GalNAc-GD1(t18:0/20:0)
1,042.66		14		
1,046.59	1,046.46	12	$[M+Na-3H]^{2-}$	GT1(d18:1/14:0) or GT1(d18:0/14:1)
1,049.62	1,049.51	10	$[M-2H]^{2-}$	GT1(d18:1/16:0) or GT1(d18:0/16:1)
1,059.61	1,059.28	31	$[M+Na-3H]^{2-}$	GT1(d18:1/16:1)
1,063.03	1,063.35	30	$[M-2H]^{2-}$	GT1(d18:1/18:0) or GT1(d18:0/18:1)
1,074.02	1,074.05	3	$[M+Na-3H]^{2-}$	GT1(d18:1/18:0)
1,077.04	1,077.37	31	$[M-2H]^{2-}$	GT1\(d18:1/20:0)
1,097.18	1,096.81	34	$M-2H]^{2-}$	*O*-Ac-GT1(d18:1/20:1) or *O*-Ac-GT1(d18:0/20:2) or *O*-Ac-GT1(d18:2/20:0)
1,097.04		21	$[M+Na-3H]^{2-}$	GT1(t18:0/20:0)
1,110.70	1,110.36	31	$[M-2H]^{2-}$	*O*-Ac-GT1(d18:1/22:2)
1,118.49	1,118.56	6	$[M-H]^{-}$	GM4(t18:1/24:0)
1,180.47	1,180.09	32	$[M-H]^{-}$	GM3(d18:1/18:0) or GM3(d18:0/18:1)
1,228.51	1,228.61	8	$[M-H]^{-}$	GA1(d18:0/16:0)
1,228.49		10	$[M+Na-2H]^{-}$	GM3(d18:1/20:1) or GM3(d18:0/20:2)
1,232.55	1,232.12	35	$[M-H]^{-}$	GM3(d18:1/22:2) or GM3(d18:0/22:3) or GM3(d18:2/22:1)
1,232.52		32	$[M+Na-2H]^{-}$	GM3(d18:0/20:0)
1,241.29	1,240.86	35	$[M+Na-3H]^{2-}$	*O*-Ac-GQ1(d18:1/18:0)

(continued)

Table 8.7 (continued)

m/z (monoisotopic) theoretical	*m/z* (monoisotopic) experimental	Mass accuracy (ppm)	Molecular ion	Proposed structure
1,252.58	1,252.19	31	$[M-H]^-$	*O*-Ac-GM3(d18:0/20:0)
1,252.60		33		GM3 (d18:0/23:0)
1,264.54	1,264.12	33	$[M-H]^-$	di-*O*-Ac-GM3(d18:1/18:0)
1,284.60	1,284.36	19	$[M+Na-2H]^-$	GM3(d18:1/24:1)
1,382.82	1,382.87	4	$[M-H]^-$	GM2(d18:1/18:0) or GM2(d18:0/18:1)
1,409.70	1,410.19	35	$[M-H]^-$	GM2(d18:1/20:0) or GM2(d18:0/20:1)
1,467.69	1,467.86	12	$[M-H]^-$	GD3(d18:1/18:2)
1,467.67		13	$[M+Na-2H]^-$	GD3(d18:0/16:0)
1,492.81	1,492.89	5	$[M+Na-2H]^-$	GD3(d18:1/18:0)
1,509.73	1,509.71	1	$[M-H]^-$	*O*-Ac-GD3(d18:1/18:1)
1,509.79		5		Fuc-GM2-lactone (d18:1/18:1)
1,513.76	1,513.29	31	$[M-H]^-$	*O*-Ac-GD3(d18:1/18:0)
1,516.84	1,517.30	30	$[M-H]^-$	GM1(d18:1/16:0) GD3(d18:2/20:2)
1,517.71		27	$[M+Na-2H]^-$	Fuc-GM2(d18:2/16:2)
1,517.70		26	$[M+Na-2H]^-$	
1,537.72	1,537.26	30	$[M+Na-2H]^-$	GM1(d18:1/16:1)
1,541.73	1,541.21	33	$[M+2Na-3H]^-$	GD3(d18:1/20:0)
1,544.87	1,544.92	3	$[M-H]^-$	GM1(d18:1/18:0) or GM1(d18:0/18:1)
1,561.80	1,561.36	28	$[M-H]^-$	*O*-Ac-GM1(d18:0/16:0)
1,566.85	1,566.68	11	$[M+Na-2H]^-$	GM1(d18:1/18:0) or GM1(d18:0/18:1)
1,572.90	1,572.92	1	$[M-H]^-$	GM1(d18:1/20:0) or GM1(d18:0/20:1)
1,589.83	1,589.28	35	$[M-H]^-$	Fuc-GD3(d18:1/16:0)
1,593.82	1,594.16	21	$[M+Na-2H]^-$	GM1(d18:1/20:0)
1,599.89	1,600.23	21	$[M-H]^-$	GM1(d18:0/22:0)
1,629.88	1,629.32	34	$[M-H]^-$	di-*O*-Ac-GM1(d18:1/18:0)
1,648.88	1,648.32	34	$[M-H]^-$	GD2(d18:0/16:0)
1,656.90	1,656.88	1	$[M-H]^-$	GD2-lactone (d18:1/18:0)

1,662.82	1,663.16	20	$[M+Na-2H]^-$	GD2(d18:2/16:2)
1,674.92	1,674.33	35	$[M-H]^-$	GD2(d18:1/18:0) or GD2(d18:0/18:1)
1,690.93	1,690.95	1	$[M-H]^-$	Fuc-GM1(d18:1/18:0)
1,700.96	1,701.42	27	$[M-H]^-$	GD2(d18:1/20:0) or GD2(d18:0/20:1)
1,708.88	1,709.36	27	$[M+Na-2H]^-$	*O*-Ac-GD2 (d18:1/16:1)
1,716.94	1,716.91	2	$[M-H]^-$	Fuc-GM1 (d18:1/20:1)
1,717.98	1,718.48	29	$[M-H]^-$	Fuc-GM1 (d18:1/20:0)
1,729.01	1,729.62	35	$[M-H]^-$	GD2(d18:1/22:0) or GD2(d18:0/22:1)
1,741.87	1,741.27	34	$[M+Na-2H]^-$	Fuc-GM1 (d18:0/20:0)
1,746.92	1,746.38	31	$[M+2Na-3H]^-$	GD2(d18:0/20:0)
1,775.04	1,775.57	30	$[M+Na-2H]^-$	GD2(d18:2/24:3)
1,787.98	1,787.76	12	$[M+2Na-3H]^-$	Fuc-GM1(d18:1/22:1)
1,796.07	1,796.50	24	$[M+Na-2H]^-$	Fuc-GM1(d18:1/24:0)
1,803.02	1,803.64	34	$[M-H]^-$	*O*-Ac-GT3(d18:1/18:1)
1,835.96	1,835.91	3	$[M-H]^-$	GD1(d18:1/18:0) or GD1(d18:0/18:1)
1,857.02	1,857.59	31	$[M+Na-2H]^-$	GD1(d18:0/18:0)
1,863.10	1,863.61	27	$[M-H]^-$	GD1(d18:1/20:0)
1,873.07	1,872.68	21	$[M+Na-2H]^-$	GD1(d18:1/19:0)
1,879.93	1,879.91	1	$[M+2Na-3H]^-$	GD1(d18:1/18:0)
1,887.79	1,886.98	5	$[M-H]^-$	Fuc-GT3-lactone(d18:1/18:2) Fuc-GT3-lactone(d18:0/18:3) Fuc-GT3-lactone(d18:2/18:1)
1,895.96	1,896.06	5	$[M+2Na-3H]^-$	GD1(d18:0/19:0)
1,901.05	1,901.71	35	$[M+2Na-3H]^-$	*O*-Ac-GT3(d18:1/22:1)
1,910.07	1,909.43	34	$[M-H]^-$	GT2(d18:0/14:0) or GT2(d18:0/14:1)
1,915.17	1,915.78	31	$[M-H]^-$	GD1(d18:1/24:2)
1,925.14	1,925.77	33	$[M+Na-2H]^-$	GD1(d18:1/23:1)
1,937.15	1,937.80	34	$[M+Na-2H]^-$	GD1(d18:1/24:2) or GD1(d18:0/24:3) or GD1(d18:2/24:1)
1,964.16	1,964.84	35	$[M-H]^-$	GT2(d18:0/18:0)

(continued)

Table 8.7 (continued)

m/z (monoisotopic) theoretical	*m/z* (monoisotopic) experimental	Mass accuracy (ppm)	Molecular ion	Proposed structure
1,983.20	1,982.55	33	$[M-H]^-$	Fuc-GD1(d18:1/18:0)
2,005.20	2,004.61	30	$[M-H]^-$	Fuc-GD1(d18:1/20:2)
2,010.16	2,010.78	31	$[M+Na-2H]^-$	GT2(d18:1/20:2) or GT2(d18:0/20:3) or GT2(d18:2/20:1)
2,032.23	2,032.63	20	$[M-H]^-$	*O*-Ac-GT2(d18:1/20:1) or *O*-Ac-GT2(d18:0/20:2) or *O*-Ac-GT2(d18:2/20:0)
2,032.14		24	$[M+2Na-3H]^-$	GT2(d18:1/20:2) or GT2(d18:0/20:3) or GT2(d18:2/20:1)
2,050.24	2,049.75	24	$[M-H]^-$	di-*O*-Ac-GT2 (d18:1/18:0)
2,059.27	2,059.78	29	$[M+Na-2H]^-$	Fuc-GD1(d18:1/22:0)
2,076.24	2,076.85		$[M-H]^-$	GQ3(d18:1/20:2) or GQ3(d18:0/20:3) or GQ3(d18:2/20:1)
2,106.27	2,105.78	23	$[M-H]^-$ $(-H_2O)$	GT1(d18:1/18:2)
2,166.32	2,165.56	35	$[M-H]^-$	*O*-Ac-GT1(d18:1/18:2) or *O*-Ac-GT1(d18:0/18:3) or *O*-Ac-GT1(d18:2/18:1)
2,165.03		24	$[M+Na-2H]^-$	GT1(t18:1/18:0)
2,166.29		34		*O*-Ac-GT1(d18:1/16:0)
2,172.19	2,172.04	7	$[M+2Na-3H]^-$	*O*-Ac-GT1(t18:1/14:1)
2,188.38	2,187.62	35	$[M+Na-2H]^-(H_2O)$	GT1(d18:1/22:0)
2,188.39		35	$[M+Na-2H]^-$	GT1(d18:1/21:1)
2,198.31	2,198.08	10	$[M+2Na-3H]^-$	GT1(d18:1/20:0)
2,214.25	2,215.78	24	$[M+Na-2H]^-$	*O*-Ac-GT1(d18:1/20:2)

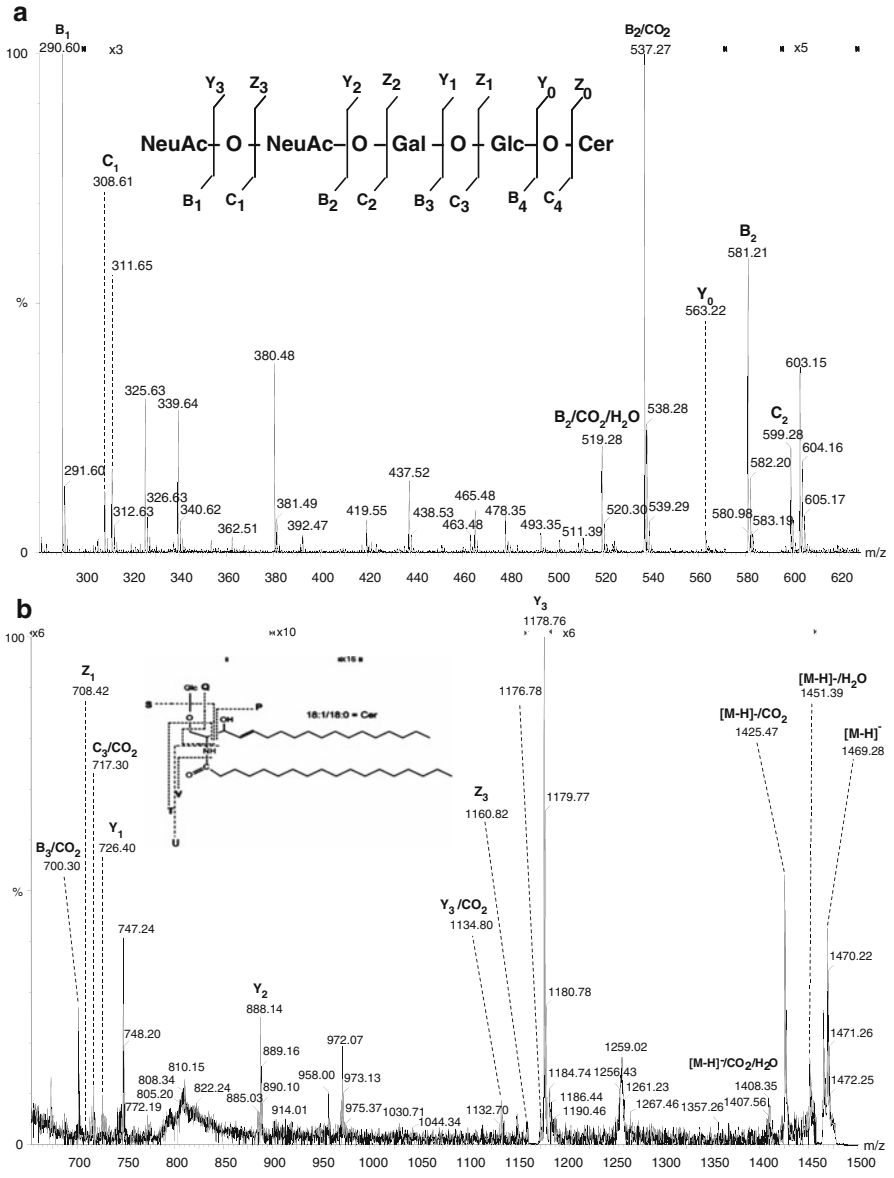

Fig. 8.17 NanoESI chip QTOF CID MS/MS of the singly charged ion at *m/z* 1,471.29 corresponding to GD3 (d18:1/18:0) from brain metastasis of lung adenocarcinoma. *m/z* range (**a**) 200–630. (**b**) 650–1,500. Acquisition time 1 min. *Insets*: fragmentation schemes of the oligosaccharide core and ceramide moiety. Reprinted with permission from Zamfir et al. [89]

The bioanalytical platforms based on mass spectrometry demonstrated here for the discovery of glycolipid/ganglioside molecular markers of brain in health and disease have real perspectives of development into routine, ultrafast, and sensitive methods applicable to other molecular markers of the pathologies at the neurological and other levels.

Acknowledgments This work was supported by the Romanian National Authority for Scientific Research, CNCS-UEFISCDI, projects PN-II-ID-PCE-2011-3-0047 PN-II-RU-2011-TE-0008 and PN-II-PCCA-2011-142 and by EU Commission, project FP7 Marie Curie-PIRSES-"MS-Life"-2010-269-256.

References

1. Almeida R, Mosoarca C, Chirita M et al (2008) Coupling of fully automated chip-based electrospray ionization to high-capacity ion trap mass spectrometer for ganglioside analysis. Anal Biochem 378:43–52
2. Ammirati M, Cobbs CS, Linskey ME et al (2010) The role of retreatment in the management of recurrent/progressive brain metastases: a systematic review and evidence-based clinical practice guideline. J Neurooncol 96:85–96
3. Augustinsson LE, Blennow K, Blomstrand C et al (1997) Intracerebroventricular administration of GM1 ganglioside to presenile Alzheimer patients. Dement Geriatr Cogn Disord 8:26–33
4. Bagce HF, Saleh S, Adamovich SV, Tunik E (2012) Visuomotor gain distortion alters online motor performance and enhances primary motor cortex excitability in patients with stroke. Neuromodulation 15:361–369
5. Birks SM, Danquah JO, King L et al (2011) Targeting the GD3 acetylation pathway selectively induces apoptosis in glioblastoma. Neuro Oncol 13:950–960
6. Bleich-Cohen M, Hendler T, Weizman R et al (2013) Working memory dysfunction in schizophrenia patients with obsessive-compulsive symptoms: an fMRI study. Eur Psychiatry 29(3): 160–166
7. Cameron M, Moran P (2009) Prenatal screening and diagnosis of neural tube defects. Prenat Diagn 29:402–411
8. Cannella MS, Oderfeld-Nowak B, Gradkowska M et al (1990) Derivatives of ganglioside GM1 as neuronotrophic agents: comparison of in vivo and in vitro effects. Brain Res 513:286–294
9. Chahlavi A, Rayman P, Richmond AL et al (2005) Glioblastomas induce T-lymphocyte death by two distinct pathways involving gangliosides and CD70. Cancer Res 65:5428–5538
10. Colorado RA, Shukla K, Zhou Y et al (2012) Multi-task functional MRI in multiple sclerosis patients without clinical disability. Neuroimage 59:573–581
11. Di Pietro F, McAuley JH, Parkitny L et al (2013) Primary somatosensory cortex function in complex regional pain syndrome: a systematic review and meta-analysis. J Pain 14:1001–1018
12. Di Pietro F, McAuley JH, Parkitny L et al (2013) Primary motor cortex function in complex regional pain syndrome: a systematic review and meta-analysis. J Pain 14:1270–1288
13. Diaz Y, Gonzalez A, Lopez A et al (2009) Anti-ganglioside anti-idiotypic monoclonal antibody-based cancer vaccine induces apoptosis and antiangiogenic effect in a metastatic lung carcinoma. Cancer Immunol Immunother 58:1117–1128
14. Domon B, Costello CE (1988) A systematic nomenclature for carbohydrate fragmentation in FAB-MS/MS spectra of glycoconjugates. Glycoconj J 5:397–409
15. Egge H, Peter-Katalinić J, Reuter G et al (1985) Analysis of gangliosides using fast atom bombardment mass spectrometry. Chem Phys Lipids 37:127–141

16. Fish RG (1996) Role of gangliosides in tumour progression: a molecular target for cancer therapy? Med Hypotheses 46:140–144
17. Flangea C, Serb A, Sisu E et al (2011) Chip-based nanoelectrospray mass spectrometry of brain gangliosides. Biochim Biophys Acta 1811:513–535
18. Flangea C, Fabris D, Vukelić Ž et al (2013) Mass spectrometry of gangliosides from human sensory and motor cortex. Aust J Chem 66:781–790
19. Fredman P, Hedberg K, Brezicka T (2003) Gangliosides as therapeutic targets for cancer. BioDrugs 17:155–167
20. Gaspar LE, Mehta MP, Patchell RA et al (2010) The role of whole brain radiation therapy in the management of newly diagnosed brain metastases: a systematic review and evidence based clinical practice guideline. J Neurooncol 96:17–32
21. Grahn JA, Parkinson JA, Owen AM (2008) The cognitive functions of the caudate nucleus. Prog Neurobiol 86:141–155
22. Gow CH, Chien CR, Chang YL (2008) Radiotherapy in lung adenocarcinoma with brain metastases: effects of activating epidermal growth factor receptor mutations on clinical response. Clin Cancer Res 14:162–168
23. Hakomori S, Handa K (2002) Glycosphingolipid-dependent cross-talk between glycosynapses interfacing tumor cells with their host cells: essential basis to define tumor malignancy. FEBS Lett 531:88–92
24. Hallinan JT, Hegde AN, Lim WE (2013) Dilemmas and diagnostic difficulties in meningioma. Clin Radiol 68:837–844
25. Han SJ, Yang I, Tihan T et al (2010) Primary gliosarcoma: key clinical and pathologic distinctions from glioblastoma with implications as a unique oncologic entity. J Neurooncol 96:313–320
26. Handa K, Hakomori SI (2012) Carbohydrate to carbohydrate interaction in development process and cancer progression. Glycoconj J 29:627–637
27. Hedberg KM, Mahesparan R, Read TA et al (2001) The glioma-associated gangliosides 3′-isoLM1, GD3 and GM2 show selective area expression in human glioblastoma xenografts in nude rat brains. Neuropathol Appl Neurobiol 27:451–464
28. Hegde AN, Mohan S, Lim CC (2012) CNS cavernous haemangioma: “popcorn” in the brain and spinal cord. Clin Radiol 67:380–388
29. Huffman K (2012) The developing, aging neocortex: how genetics and epigenetics influence early developmental patterning and age-related change. Front Genet 3:212–220
30. IUPAC-IUB Joint Commission on Biochemical Nomenclature (1998) Nomenclature of glycolipids. Eur J Biochem 257:293–298
31. Kaas JH (2012) The evolution of neocortex in primates. Prog Brain Res 195:91–102
32. Kalanj S, Kracun I, Rosner H, Cosović C (1991) Regional distribution of brain gangliosides in Alzheimer’s disease. Neurol Croat 40:269–281
33. Kniep B, Kniep E, Ozkucur N et al (2006) 9-O-acetyl GD3 protects tumor cells from apoptosis. Int J Cancer 119:67–73
34. Kojovic M, Bologna M, Kassavetis P et al (2012) Functional reorganization of sensorimotor cortex in early Parkinson disease. Neurology 78:1441–1448
35. Kracun I, Kalanj S, Talan-Hranilovic J et al (1992) Cortical distribution of gangliosides in Alzheimer’s disease. Neurochem Int 20:433–438
36. Krafft C, Neudert L, Simat T et al (2005) Near infrared Raman spectra of human brain lipids. Spectrochim Acta A Mol Biomol Spectrosc 61:1529–1535
37. Kroes RA, He H, Emmett MR et al (2010) Overexpression of ST6GalNAcV, a ganglioside-specific alpha2,6-sialyltransferase, inhibits glioma growth in vivo. Proc Natl Acad Sci U S A 107:12646–12651
38. Lefebvre L (2012) Primate encephalization. Prog Brain Res 195:393–412
39. Lehnhardt FG, von Smekal U, Rűckriem B et al (2005) Value of gradient-echo magnetic resonance imaging in the diagnosis of familial cerebral cavernous malformation. Arch Neurol 62:653–658

40. Levery SB (2005) Glycosphingolipid structural analysis and glycosphingolipidomics. Methods Enzymol 405:300–369
41. Lode HN, Schmidt M, Seidel D et al (2013) Vaccination with anti-idiotype antibody ganglidiomab mediates a GD(2)-specific anti-neuroblastoma immune response. Cancer Immunol Immunother 62:999–1010
42. Louis David N, Hiroko O, Wiestler D (2007) The 2007 WHO classification of tumours of the central nervous system. Acta Neuropathol 114:97–109
43. Lukas RV, Nicholas MK (2013) Update in the treatment of high-grade gliomas. Neurol Clin 31:847–867
44. Lutterbach J, Guttenberger R, Pagenstecher A (2001) Gliosarcoma: a clinical study. Radiother Oncol 61:57–64
45. Meck WH, Church RM, Matell MS (2013) Hippocampus, time, and memory—a retrospective analysis. Behav Neurosci 127:642–654
46. Messner MC, Cabot MC (2010) Glucosylceramide in humans. Adv Exp Med Biol 688:156–164
47. Mitsuzuka K, Handa K, Satoh M et al (2005) A specific microdomain ("glycosynapse 3") controls phenotypic conversion and reversion of bladder cancer cells through GM3-mediated interaction of alpha3beta1 integrin with CD9. J Biol Chem 280:35545–35553
48. Mochizuki Y, Mizutani T, Shimizu T et al (2011) Proportional neuronal loss between the primary motor and sensory cortex in amyotrophic lateral sclerosis. Neurosci Lett 503:73–75
49. Mosoarca C, Ghiulai RM, Novaconi CR et al (2011) Application of chip-based nanoelectrospray ion trap mass spectrometry to compositional and structural analysis of gangliosides in human fetal cerebellum. Anal Lett 44:1036–1049
50. Nelles G, Jentzen W, Bockisch A et al (2011) Neural substrates of good and poor recovery after hemiplegic stroke: a serial PET study. J Neurol 258:2168–2175
51. Noguchi M, Suzuki T, Kabayama K et al (2007) GM3 synthase gene is a novel biomarker for histologic classification and drug sensitivity against epidermal growth factor receptor tyrosine kinase inhibitors in non-small-cell lung cancer. Cancer Sci 98:1625–1632
52. Oikawa N, Yamaguchi H, Ogino K et al (2009) Gangliosides determine the amyloid pathology of Alzheimer's disease. Neuroreport 20:1043–1046
53. Park Y, Lebrilla CB (2005) Application of Fourier transform ion cyclotron resonance mass spectrometry to oligosaccharides. Mass Spectrom Rev 24:232–264
54. Pellizzaro Venti M, Paciaroni M et al (2012) Caudate infarcts and hemorrhages. Front Neurol Neurosci 30:137–140
55. Pernber Z, Blennow K, Bogdanovic N et al (2012) Altered distribution of the gangliosides GM1 and GM2 in Alzheimer's disease. Dement Geriatr Cogn Disord 33:174–188
56. Relini A, Marano N, Gliozzi A (2013) Probing the interplay between amyloidogenic proteins and membranes using lipid monolayers and bilayers. Adv Colloid Interface Sci. doi:10.1016/j.cis.2013.10.015
57. Rodriguez FJ, Lim KS, Bowers D et al (2013) Pathological and molecular advances in pediatric low-grade astrocytoma. Annu Rev Pathol 8:361–379
58. Ryan JM, Rice GE, Mitchell MD (2013) The role of gangliosides in brain development and the potential benefits of perinatal supplementation. Nutr Res 33:877–887
59. Sandhoff K, Harzer K (2013) Gangliosides and gangliosidoses: principles of molecular and metabolic pathogenesis. J Neurosci 33:10195–10208
60. Santin AD, Ravindranath MH, Bellone S et al (2004) Increased levels of gangliosides in the plasma and ascitic fluid of patients with advanced ovarian cancer. BJOG 111:613–618
61. Schiopu C, Flangea C, Capitan F et al (2009) Determination of ganglioside composition and structure in human brain hemangioma by chip-based nanoelectrospray ionization tandem mass spectrometry. Anal Bioanal Chem 395:2465–2477
62. Schiopu C, Vukelić Z, Capitan F et al (2012) Chip-nanoelectrospray quadrupole time-of-flight tandem mass spectrometry of meningioma gangliosides: a preliminary study. Electrophoresis 33:1778–1786

63. Schneider JS, Sendek S, Daskalakis C et al (2010) GM1 ganglioside in Parkinson's disease: results of a five year open study. J Neurol Sci 292:45–51
64. Schneider JS, Gollomp SM, Sendek S et al (2013) A randomized, controlled, delayed start trial of GM1 ganglioside in treated Parkinson's disease patients. J Neurol Sci 324:140–148
65. Serb A, Sisu E, Vukelić Z et al (2012) Profiling and sequencing of gangliosides from human caudate nucleus by chip-nanoelectrospray mass spectrometry. J Mass Spectrom 47:1561–1570
66. Seyfried TN, Mukherjee P (2010) Ganglioside GM3 is antiangiogenic in malignant brain cancer. J Oncol 2010:961243
67. Shibuya H, Hamamura K, Hotta H et al (2012) Enhancement of malignant properties of human osteosarcoma cells with disialyl gangliosides GD2/GD3. Cancer Sci 103:1656–1664
68. Shukla GS, Krag DN (2006) Selective delivery of therapeutic agents for the diagnosis and treatment of cancer. Expert Opin Biol Ther 6:39–54
69. Sisu E, Flangea C, Serb A et al (2011) High-performance separation techniques hyphenated to mass spectrometry for ganglioside analysis. Electrophoresis 32:1591–1609
70. Steiner G, Shaw A, Choo-Smith LP et al (2003) Distinguishing and grading human gliomas by IR spectroscopy. Biopolymers 72:464–471
71. Svennerholm L, Fredman P (1980) A procedure for the quantitative isolation of brain gangliosides. Biochim Biophys Acta 617:97–109
72. Taki T (2012) An approach to glycobiology from glycolipidomics: ganglioside molecular scanning in the brains of patients with Alzheimer's disease by TLC-blot/matrix assisted laser desorption/ionization-time of flight MS. Biol Pharm Bull 35:1642–1647
73. Tang T, Kmet M, Corral L et al (2005) Testisin, a glycosyl-phosphatidylinositol-linked serine protease, promotes malignant transformation in vitro and in vivo. Cancer Res 65:868–878
74. Tivnan A, Orr WS, Gubala V et al (2012) Inhibition of neuroblastoma tumor growth by targeted delivery of microRNA-34a using anti-disialoganglioside GD2 coated nanoparticles. PLoS One 7:e38129
75. Tokuda N, Zhang Q, Yoshida S (2006) Genetic mechanisms for the synthesis of fucosyl GM1 in small cell lung cancer cell lines. Glycobiology 16:916–925
76. Yamazaki T, Suzuki M, Irie T et al (2008) Amyotrophic lateral sclerosis associated with IgG anti-GalNAc-GD1a antibodies. Clin Neurol Neurosurg 110:722–724
77. Yu RK, Tsai YT, Ariga T (2012) Functional roles of gangliosides in neurodevelopment: an overview of recent advances. Neurochem Res 37:1230–1244
78. Valdes-Gonzalez T, Goto-Inoue N et al (2011) New approach for glyco- and lipidomics-molecular scanning of human brain gangliosides by TLC-Blot and MALDI-QIT-TOF MS. J Neurochem 116:678–683
79. Vriend C, Raijmakers P, Veltman DJ et al (2014) Depressive symptoms in Parkinson's disease are related to reduced [123I]FP-CIT binding in the caudate nucleus. J Neurol Neurosurg Psychiatry 85(2):159–164
80. Vukelić Z, Metelmann W, Müthing J et al (2001) Anencephaly: structural characterization of gangliosides in defined brain regions. Biol Chem 382:259–274
81. Vukelić Z, Zamfir AD, Bindila L et al (2005) Screening and sequencing of complex sialylated and sulfated glycosphingolipid mixtures by negative ion electrospray Fourier transform ion cyclotron resonance mass spectrometry. J Am Soc Mass Spectrom 16:571–580
82. Vukelić Z, Zarei M, Peter-Katalinić J et al (2006) Analysis of human hippocampus gangliosides by fully-automated chip-based nanoelectrospray tandem mass spectrometry. J Chromatogr A 1130:238–245
83. Vukelić Z, Kalanj-Bognar S, Froesch M et al (2007) Human gliosarcoma-associated ganglioside composition is complex and distinctive as evidenced by high-performance mass spectrometric determination and structural characterization. Glycobiology 17:504–515
84. Wagener R, Röhn G, Schillinger G et al (1999) Ganglioside profiles in human gliomas: quantification by microbore high performance liquid chromatography and correlation to histomorphology and grading. Acta Neurochir (Wien) 141:1339–13345

85. Walcott BP, Nahed BV, Brastianos PK et al (2013) Radiation treatment for WHO grade II and III meningiomas. Front Oncol 3:227
86. Walker FO (2007) Huntington's disease. Lancet 369:218
87. Wessels PH, Weber WE, Raven G et al (2003) Supratentorial grade II astrocytoma: biological features and clinical course. Lancet Neurol 2:395–403
88. Zamfir AD, Vukelić Z, Bindila L et al (2004) Fully-automated chip-based nanoelectrospray tandem mass spectrometry of gangliosides from human cerebellum. J Am Soc Mass Spectrom 15:1649–1657
89. Zamfir AD, Serb A, Vukelić Ž et al (2011) Assessment of the molecular expression and structure of gangliosides in brain metastasis of lung adenocarcinoma by an advanced approach based on fully automated chip-nanoelectrospray mass spectrometry. J Am Soc Mass Spectrom 22:2145–2159
90. Zamfir AD, Fabris D, Capitan F et al (2013) Profiling and sequence analysis of gangliosides in human astrocytoma by high-resolution mass spectrometry. Anal Bioanal Chem 405:7321–7335
91. Zhang Q, Furukawa K, Chen HH et al (2006) Metastatic potential of mouse Lewis lung cancer cells is regulated via ganglioside GM1 by modulating the matrix metalloprotease-9 localization in lipid rafts. J Biol Chem 281:18145–18155